

Potentially Wearable Thermo-Electrochemical Cells for Body Heat Harvesting: From Mechanism, Materials, Strategies to Applications

Yuqing Liu, Hongbo Wang,* Peter C. Sherrell, Lili Liu, Yong Wang, and Jun Chen*

Wearable electronics are becoming one of the key technologies in health care applications including health monitoring, data acquisitions, and real-time diagnosis. The commercialization of next-generation devices has been stymied by the lack of ultrathin, flexible, and reliable power sources. Wearable thermo-electrochemical cells (TECs), which can convert body heat to electricity via an electrochemical process, are showing great promise as power sources for such wearable systems. TECs harvest orders of magnitude more voltage per temperature difference (Seebeck coefficient ($1\text{--}34\text{ mV K}^{-1}$)) when compared to the more common thermoelectric generators (Seebeck coefficient \approx tens or hundreds of $\mu\text{V K}^{-1}$). However, there still remain great challenges for TECs progressing towards wearable applications. This review summarizes the recent development of potentially wearable TECs with promise for body-heat harvesting, with a specific focus on flexible electrode materials, solid-state electrolytes, device fabrication, and strategies toward applications. It also clarifies the challenges and gives some future direction to enhance future investigations on high-performance wearable TECs for practical and self-powered wearable devices.

1. Introduction

Wearable electronic systems are becoming one of the key technologies in healthcare applications including health monitoring, wireless data acquisitions and transfers, and real-time diagnosis. The emergence of wearable electronics needs for power supply systems that are light, flexible, and user friendly.^[1–5] As the alternative to energy storage systems (including batteries^[6–11] and supercapacitors^[12–14]), self-powered systems that harvest energy from the human body or the outside environment (e.g., solar,^[15,16] mechanical energy^[17–19]) is attracting increasing attention from researchers. These self-powered systems use energy that is environmentally friendly and sustainable, with recent developments in advanced wearable energy conversion devices enabling efficient power extraction from users (especially the elderly).^[20–23] For example, solar cells are widely applied, and

show the greatest potential among energy conversion devices, with the latest advances surrounding flexible and stretchable solar cells.^[15,24,25] The fast growth of piezoelectric and triboelectric generator devices, driven by improved mechanistic understanding,^[26,27] has led to the emergence of self-powered systems via harvesting mechanical energy from the human movement.^[28–32] However, these energy harvesting strategies rely on either the exposure to sunlight or the circumstances when human movement exists, limiting the opportunity for energy harvesting.^[1]


Alternatively, human body heat is considered a promising source of constant energy, which could fill the gap of solar and mechanical energy harvesting.^[33,34] Our human body can continually provide thermal energy up to 20 mW cm^{-2} and there is always a temperature difference between the skin and the outside environment.^[1,33,34] To harvest this energy, thermoelectric generators (TEG) were first studied. Owing to the recent development of organic thermoelectric (TE) materials, flexible and even stretchable TEGs prototypes were gradually reported, where the Seebeck coefficient ($S_e = \Delta V/\Delta T$) was greatly limited to tens of $\mu\text{V K}^{-1}$.^[35–38] The converted voltage output from low-grade body heat (where ΔT is in the range of $5\text{ }^\circ\text{C}$ – $10\text{ }^\circ\text{C}$) is thus far from the requirement of wearable electronics (the order of hundreds of mV to several V) unless in series connecting hundreds of single devices together.^[35–38]

Dr. Y. Liu, Dr. H. Wang, Dr. Y. Wang
State Key Laboratory of Electronic Thin Film and Integrated Devices
University of Electronic Science and Technology of China
Chengdu 610054, P. R. China
E-mail: hongbowang@uestc.edu.cn

Dr. P. C. Sherrell
Department of Chemical Engineering
University of Melbourne
Melbourne VIC 3010, Australia

Dr. L. Liu
School of Energy and Institute for Advanced Materials
Nanjing Tech University
Jiangsu Province Nanjing 211816, China

Prof. J. Chen
Intelligent Polymer Research Institute and ARC Centre of Excellence for Electromaterials Science
Australian Institute for Innovative Materials
University of Wollongong
Wollongong NSW 2500, Australia
E-mail: junc@uow.edu.au

 The ORCID identification number(s) for the author(s) of this article can be found under <https://doi.org/10.1002/advs.202100669>

© 2021 The Authors. Advanced Science published by Wiley-VCH GmbH. This is an open access article under the terms of the Creative Commons Attribution License, which permits use, distribution and reproduction in any medium, provided the original work is properly cited.

DOI: 10.1002/advs.202100669

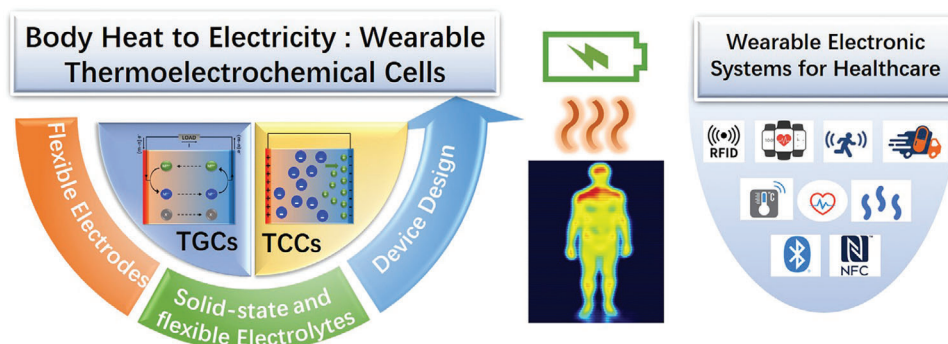


Figure 1. Schematic illustration of the current directions in developing wearable thermo-electrochemical cells and the potential applications in wearable electronic systems for healthcare.

Thermo-electrochemical cells (TECs), which can convert heat to electricity via the temperature dependence of the electrochemical process, display Seebeck coefficients hundreds of times higher than flexible TEGs.^[39–41] This high performance, coupled to cheap and environmentally friendly electrode and electrolyte materials and simple device construction, is leading to increasing interest in TECs for low-grade heat harvesting. While all TECs have the same basic configuration of two electrodes sandwiching an electrolyte, there exist multiple subclasses of TECs defined by their different operating mechanisms including thermogalvanic cells (TGCs),^[41–44] thermally chargeable capacitors (TCCs),^[45–47] and thermally regenerative batteries.^[48,49] These subcategories of TECs features key advantages that can aid in application specificity in terms of energy output consistency, maximum output voltage, or conversion efficiency. Meanwhile, each possesses its challenges in designing feasible devices to supply power for wearable applications.

This article presents an overview of the recent advances of wearable TECs in terms of flexible electrodes, solid-state and flexible electrolytes, and device design (Figure 1). We summarize the development and potential of TECs in wearable applications for body heat harvesting, make comparisons, clarify the challenges and provide future directions for each type of TEC, focused on improving the overall output performance for wearable applications and self-powered wearable systems.

2. Potential Wearable Thermogalvanic Cells

2.1. Thermogalvanic Cells

The configuration and mechanism of a thermogalvanic cell (TGC) is illustrated in Figure 2, which shows a TGC consists of two identical electrodes with an electrolyte containing redox couples. When a temperature gradient is applied across the cell, temperature-dependent redox reactions between redox couples (e.g., M^{m+} and M^{n+}) will take place at the electrode/electrolyte interfaces, forming the potential difference between the two electrodes. Once the two electrodes are connected with the external load, the charge on the electrode materials provided from the redox reaction can flow through the external circuit. Meanwhile, the redox species consumed on one electrode will be supplanted through migration from the other electrode where the reverse re-

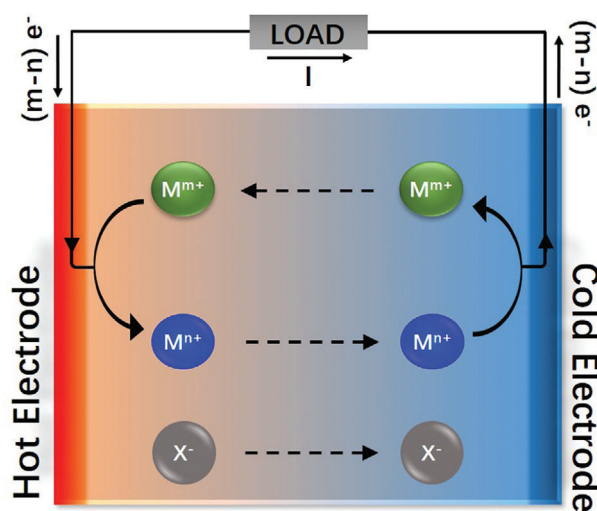


Figure 2. The configuration and working mechanism of a TGC device.

action is occurring, keeping continuity of the reaction and thus electricity generation.^[41]

The potential difference generated in the cell is dependent on the reaction entropy of redox couples across the cell. If the redox reaction in TCCs is:



If we define M^{m+} and M^{n+} as A and B respectively, the Seebeck coefficient S_e (thermally generated voltage per temperature difference) is given by:

$$\begin{aligned} S_e &= \frac{\partial V}{\partial T} = \frac{V_{\text{hot}} - V_{\text{cold}}}{T_{\text{hot}} - T_{\text{cold}}} \\ &= \frac{(S_B + \hat{S}_B) - (S_A + \hat{S}_A) - n\bar{S}_e}{nF} \approx \frac{S_B - S_A}{nF} \end{aligned} \quad (2)$$

where V is the voltage generated across the two electrodes, n is the number of electrons involved in the reaction, F is Faraday's constant, S_A and S_B are the partial molar entropies of species A and species B, and their respective Eastman entropies are denoted by \hat{S}_A and \hat{S}_B , accordingly, \bar{S}_e is the transported entropy of the

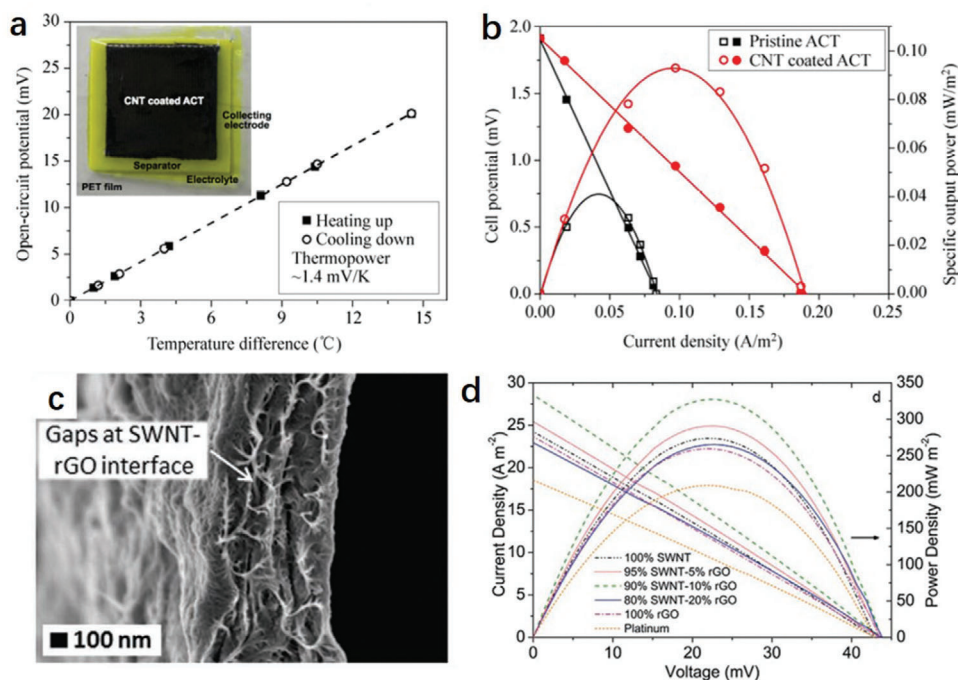


Figure 3. a) Dependence of open-circuit potential on the temperature difference between hot and cold C-ACT electrode (Inset: Photograph of the plastic thermocell). b) Thermocell discharge and specific output power as a function of the current density of the pristine ACT and C-ACT electrodes. a,b) Reproduced with permission.^[75] Copyright 2015, Tsinghua University Press and Springer. c) Cross-sectional SEM image of 90% SWNT–10% rGO composite and d) Current density versus voltage and power density versus voltage generated using various electrode compositions at $\Delta T = 31$ °C. Reproduced with permission.^[78] Copyright 2013, Wiley-VCH.

electrons in the external circuit. In most cases the Eastman entropy and \bar{S}_e is negligible compared to \bar{S}_A and \bar{S}_B , so the S_e is mainly dependent on the partial molar entropies of species A and species B, which is determined by the chemical nature of redox couples and the surrounding solvent environments.^[41,50]

Most of the current investigations on TGCs are based on the liquid electrolyte system, where the p-type redox couples of $\text{Fe}(\text{CN})_6^{3-/4-}$ ^[51,52] and n-type redox couples like I^-/I_3^- ^[53–55] $\text{Fe}^{2+}/\text{Fe}^{3+}$ ^[54,56,57] $\text{Co}^{\text{II/III}}(\text{bpy})_3^{2+/3+}$ ^[58,59] are the most commonly investigated due to the large entropy change between oxidants and reductants in solvents. The definition of p/n type for redox couples originates from that of thermoelectric materials.^[60] Specifically, the redox couple has a negative (or positive) sign indicates that the hot electrode behaves as the anode, which is analogous to a p-doped (or n-doped) thermoelectric and defined as p-type (or n-type) redox couple.^[60] To amplify the entropy change of redox couples for a high S_e , efforts have focused on; varying the solvation shell of the redox active species by using different solvent systems (e.g., water,^[42,61] organic solvents,^[59] ionic liquids^[53,59] or their mixtures^[62]); the incorporation of additives (like chaotropic cations for $\text{Fe}(\text{CN})_6^{3-/4-}$ ^[63] and α -cyclodextrins for I^-/I_3^- ^[64–66]); and employing different counter ions, such as Cl^- , SO_4^{2-} , NO_3^- , ClO_4^- for $\text{Fe}^{2+/3+}$ ^[57,67], NTf_2^- and Cl^- for $\text{Co}^{\text{II/III}}(\text{bpy})_3^{2+/3+}$.^[68]

In addition to the S_e , the exchange current density is also important to achieve the high-power output of TGCs. Generally, the exchange current density is dependent on the ion concentration and diffusion coefficient of electrolytes,^[60,67] the charge transfer resistance on the interface of between the electrode/electrolyte as well as the electric transport ability of the

electrode materials.^[51,69–73] Therefore, electrode materials with the high catalytic surface, high electrical conductivity, and large surface area such as platinum, carbon materials and conducting polymers are highly promising.

2.2. Potential Materials for Wearable TGCs

2.2.1. Flexible Electrode Materials

Wearable TGCs are required to be flexible, light-weight, and soft. A key challenge is to develop such a flexible electrode without sacrificing the high-performance properties (such as the catalytic surface, high electrical conductivity, and large surface area, etc.) required for TGCs. In recent years, two main strategies have been employed to prepare such flexible electrodes, either using a relatively inflexible active material on a flexible substrate such as PET sheets, textiles, cloth, etc.,^[74–76] or alternatively developing intrinsically flexible electrode materials.^[51,77,78]

Carbon Textile or Carbon Cloth Based Electrodes: Carbon textiles or carbon cloths are good candidates as flexible substrates that also possess acceptable electronic conductivity.^[79] Kim et al. reported the first carbon textile-based electrodes (**Figure 3a,b**), where the carbon nanotubes (CNTs) are deposited onto an activated carbon textile (ACT) via a dip-coating method.^[75] They demonstrated that the CNT coated ACT (C-ACT) exhibits lower charge transfer resistance (R_{ct}), mass transport resistance (R_{mt}), and equivalent series resistance (ESR) than the pure ACT, and thereby yielding more than two times higher

thermo-electrochemical performance than the pure ACT in terms of normalized current density (139.15 vs 62.32 mA m⁻² K⁻¹) and normalized power density (48.86 vs 21.9 μW m⁻² K⁻²) in 0.4 M K_{3/4}Fe(CN)₆ electrolyte. It is worth mentioning that, using this flexible electrode, a real flexible TGCs device in harvesting body heat was reported, which will be discussed further in the device design (Section 2.3).

Instead of depositing active materials onto a purchased carbon textile or carbon cloth, Baughman et al. devoted efforts to the treatment of the purchased carbon cloth products and greatly enhanced the exchange current density and power output of TGCs.^[76] Commercial carbon cloths were modified by simple thermal annealing (1500 °C in argon) or soaking in alkaline solution (in 2 M KOH for 24 h) followed by post thermal treatment (900 °C in argon). Thermal annealing was shown to boost the electrical conductivity from 2.6 S cm⁻² to 160 S cm⁻¹, while the alkaline treatment approach enhanced the electroactive surface area (ESA), producing a porous structure and increasing the wettability to electrolytes. As a result, the activated carbon cloth (A-CC) film electrode exhibits the highest normalized power density ($P_{\max}/(\Delta T)^2$) of 1.80 mW m⁻² K⁻² in the K₃Fe(CN)₆/(NH₄)₄Fe(CN)₆ electrolytes, even surpassing that of extremely expensive platinum foil (1.38 mW m⁻² K⁻²). Despite that flexible devices are not demonstrated in this work, these flexible A-CC film electrodes show the great potential of carbon textile/cloth-based electrodes in flexible TGCs.

Intrinsically Flexible Electrode Materials: Exploring active materials that are intrinsically flexible is another effective method to achieve high-performance electrodes. The network of 1D carbon nanotubes (CNTs) usually exhibits remarkable mechanical properties in addition to excellent electrical conductivity, large surface area, and good catalytic behavior.^[80] In Ray Baughman's group, a CNT buckypaper was made from a network of multi-walled carbon nanotubes (MWNT) by vacuum filtration, which exhibited a high electrical conductivity of 100 S cm⁻¹ and a large internal surface area of 278 m² g⁻¹.^[51] The TGCs made by this MWNT buckypaper delivered a high $P_{\max}/(\Delta T)^2$ of 0.38 mW m⁻² K⁻² in 0.4 M K_{3/4}Fe(CN)₆ aqueous electrolyte, which is higher than that of a platinum electrode (0.28 mW m⁻² K⁻²). After the flexible MWNT film electrode is assembled into a flexible TGC device, and then wrapped on a cooling pipe for energy harvesting, the TGC yielding a V_{OC} of 21 mV at a ΔT of 15 °C and normalized power density of $P_{\max}/(\Delta T)^2$ of 0.18 mW m⁻² K⁻². Such flexible TGCs exhibit lower $P_{\max}/(\Delta T)^2$ than that of the Teflon TGCs may arise from the decreasing distance between electrodes (from 2.6 to 0.2 cm for flexible TGCs). The lower distance between electrodes is good for a flexible device while resulting in faster heat transfer and smaller ΔT between electrodes. How to get the electrodes closer while keeping a relatively large ΔT between them is still the main challenge of flexible TGCs nowadays.

However, the mass transport of electrolyte ions is limited through pure CNT electrodes owing to the tortuous nature.^[78] To solve this problem, Chen et al. incorporated reduced graphene oxide (rGO) into the SWNTs and achieved a higher $P_{\max}/(\Delta T)^2$ of 0.46 mW m⁻² K⁻² (Figure 3c,d).^[78] The performance enhancement is attributed to the increased porosity and low tortuosity of the composite film electrodes, which was confirmed by the increased ESA and fast electron transfer kinetics. Meanwhile, the incorporation of 2D rGO sheets induced partial

alignment into the composite film, while maintaining good flexibility.

Beyond purely carbon-based materials, conducting polymers are another promising active material for flexible electrodes, as they can exhibit flexibility, possess molecular porosity, possess an intrinsically high surface area for small reactants, and are favorable ion transport conductors.^[3,81,83] Poly(3,4-ethylenedioxythiophene)/polystyrenesulfonic acid (PEDOT/PSS) is a promising conducting polymer. Its phase structure can be changed by dopants (such as ethylene glycol,^[84] diethylene glycol,^[85] dimethyl sulfoxide,^[86] or ionic liquids^[3]) and the polymer will exhibit different electrical and electrochemical properties. Crispin et al. first reported PEDOT/PSS-based electrodes in TGCs, in which PEDOT/PSS films were treated by a secondary dopant with dimethyl sulfoxide (DMSO).^[81] After DMSO treatment of the core-shell structured (conductive PEDOT/PSS core and insulating PSS shell) PEDOT/PSS film, the excess hydrophilic PSS was separated into nanodomains and an interconnected network of highly conducting PEDOT/PSS was created (Figure 4a). This percolating PEDOT/PSS network greatly enhanced the electrical conductivity (by over three orders of magnitude from 0.4 to 805 S cm⁻¹). Owing to the fast electron transfer and good penetration of aqueous electrolytes, PEDOT/PSS-based TGCs exhibit a $P_{\max}/(\Delta T)^2$ of 0.45 mW m⁻² K⁻², which is comparable with the well-developed carbon-based electrodes and platinum electrodes.

PEDOT/PSS can also be incorporated into well-developed carbon systems (i.e., graphene or CNT film), which can alleviate the mass transport problem caused by the large tortuosity of CNTs and the sheet restacking of graphene electrodes.^[77,82,87] Chen et al. prepared a composite film electrode made by combining PEDOT/PSS, edge functionalized graphene (EFG), and CNT via a simple drop-casting method (Figure 4b).^[82] The water-dispersible PEDOT/PSS works as a dispersing and film-forming agent, in addition to providing an ion transport pathway and increasing the porosity of EFG/CNT. EFG/CNT in turn offers more catalytic surface in the composite film. Meanwhile, an additional laser-etching process was applied on the composite film, facilitating the penetration of the electrolyte and improving the effective temperature difference between the cold and hot electrode/electrolyte interface. As a result, an instantaneous high $P_{\max}/(\Delta T)^2$ of 0.72 mW m⁻² K⁻² was achieved in the viscous gel electrolyte containing 0.4 M K_{3/4}FeCN₆. They also investigated the electrodes in an n-type electrolyte of PVA-FeCl_{2/3} (1 M FeCl_{2/3}) system and suggested that pure PEDOT/PSS film exhibited superior performance of $P_{\max}/(\Delta T)^2$ of 0.38 mW m⁻² K⁻², which surpasses all other composite materials such as PEDOT/PSS-CNT, PEDOT/PSS-EFG, and PEDOT/PSS-EFG/CNT film. This was attributed to the negative charges on excess PSS in PEDOT/PSS having a particularly high affinity for multivalent cations and thus enhanced the cation transport through the polymer electrode. These results broaden the application of the flexible PEDOT/PSS electrodes in TGCs.

2.2.2. Gel Electrolyte

For practical use of thermogalvanic cells in wearable devices, as an important type of solid-state electrolytes, gel electrolytes have

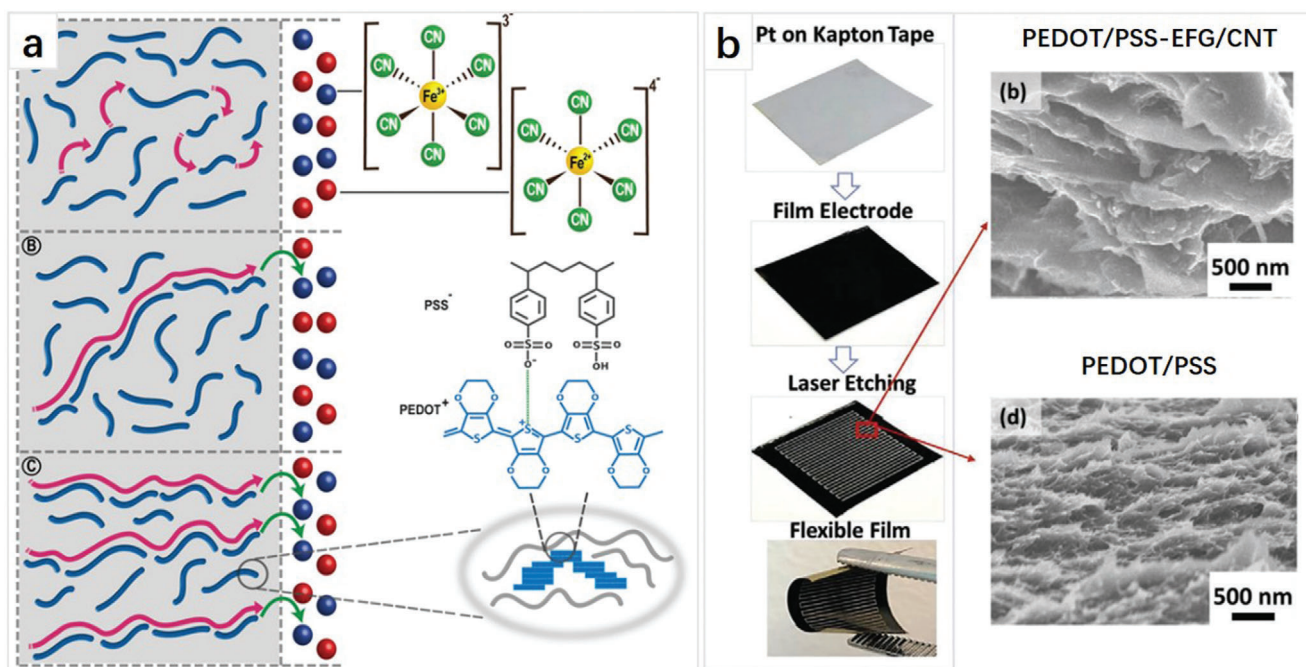


Figure 4. a) Schematic diagram of charge transport (pink arrows) within the polymer electrode and the electron transfer (green arrows) at the polymer electrolyte interface for poor-conducting (the left top one), intermediate-conducting (left-middle), and high-conducting PEDOT/PSS electrodes (left-bottom). The blue “snake” lines (on the left-hand side) mimic aggregates of PEDOT chains that display short-range order through π - π stacks. Reproduced with permission.^[81] Copyright 2018, National Academy of Sciences. b) Schematic illustration and SEM images of laser-etched PEDOT/PSS-EFG/CNT and PEDOT/PSS film electrodes. Reproduced with permission.^[82] Copyright 2020, Wiley-VCH.

been gradually developed as they avoid leakage issues of electrolytes and exhibit excellent mechanical properties of flexibility and/or stretchability.^[88] The gel electrolytes usually consist of a polymer host which can provide mechanical strength and the electrolyte containing redox couples.^[89] Both p-type and n-type redox couples have been made into these kinds of gels. The mechanical and thermo-electrochemical performance of these gels are greatly dependent on the concentration of redox couples as well as the chemical nature, molecular weight, and concentration of polymer gelling agent.^[88,89]

Gel Electrolytes Consisting of p-Type Redox Couple of $Fe(CN)_6^{3-/4-}$: $Fe(CN)_6^{3-/4-}$ is a benchmark p-type redox couple in TGCs, and in aqueous solution usually exhibits the best performance of all studied electrolytes. Therefore, great attention has been paid to develop a gel electrolyte based around the aqueous $Fe(CN)_6^{3-/4-}$ system. Due to the high chemical activity of $Fe(CN)_6^{3-/4-}$, the polymer matrix and the gelling process should be chemically inert and harmless to these reactive redox couples.

As one of the most widely used polymer hosts for gel electrolytes in supercapacitors, poly(vinyl alcohol) (PVA) gel electrolytes were a clear starting point for TGCs. Zhou et al. prepared a PVA- $K_{3/4}FeCN_6$ gel electrolyte which contained 10 wt% PVA and 0.1 M $K_{3/4}FeCN_6$ by simply mixing their solutions.^[88] The prepared gel is homogeneous, exhibits good moldability, and possessed a high mechanical strength. Despite the low concentration of redox couples and the lack of systematic investigations in this short communication, the work highlighted the potential of gel electrolytes for TGCs igniting further research.^[88]

In recent years, polyanionic polymers like poly(sodium acrylate) or carboxymethylcellulose sodium (CMC) have been proved to be a good mediator for the preparation of $K_{3/4}FeCN_6$ based gel electrolytes. These polyanionic polymer gels show compatibility with the redox couples and do not hinder redox species transport or diffusion as they do not electrostatically retain the anionic redox couple (i.e., $Fe(CN)_6^{3-/4-}$).^[89] For example, Aldous et al. prepared a polyanionic polymer-based gel electrolyte by simply mixing the 5.5 wt% poly(sodium acrylate) beads into 0.1 M $K_{3/4}FeCN_6$ solution via manual stirring and ultrasonication (Figure 5a,c).^[89] These gels show cyclic voltammetry almost identical to that of the aqueous electrolyte (0.1 M $K_{3/4}FeCN_6$) in a three-electrode system, indicating highly reversible redox chemistry and unhindered diffusion of the redox couples in a gel electrolyte. As a result, the gel electrolyte exhibits a typical thermo-electrochemical behavior with a stable Seebeck coefficient of -1.09 ± 0.04 mV K⁻¹. In this work, they also provide demonstrate examples of other polymer gelators that do not present good performance, including polysaccharide (food-grade agar agar) (Figure 5b), a protein (food-grade gelatin powder), a nanomaterial (fumed silica). Among them, gelatin gels melt at a relatively low temperature of 35 °C, while the fumed silica requires an acidic environment to form effective gels, thus they are unfavorable for $K_{3/4}FeCN_6$. Only agar agar formed a free-standing gel, which also shows a significant reduction in the current density of voltammetry curves compared with the poly (sodium acrylate) gels and aqueous electrolytes. In addition, they provide a method to determine the gelation of quasi-solid-state electrolytes through a simple “inversion” test method, where the sample is in the container

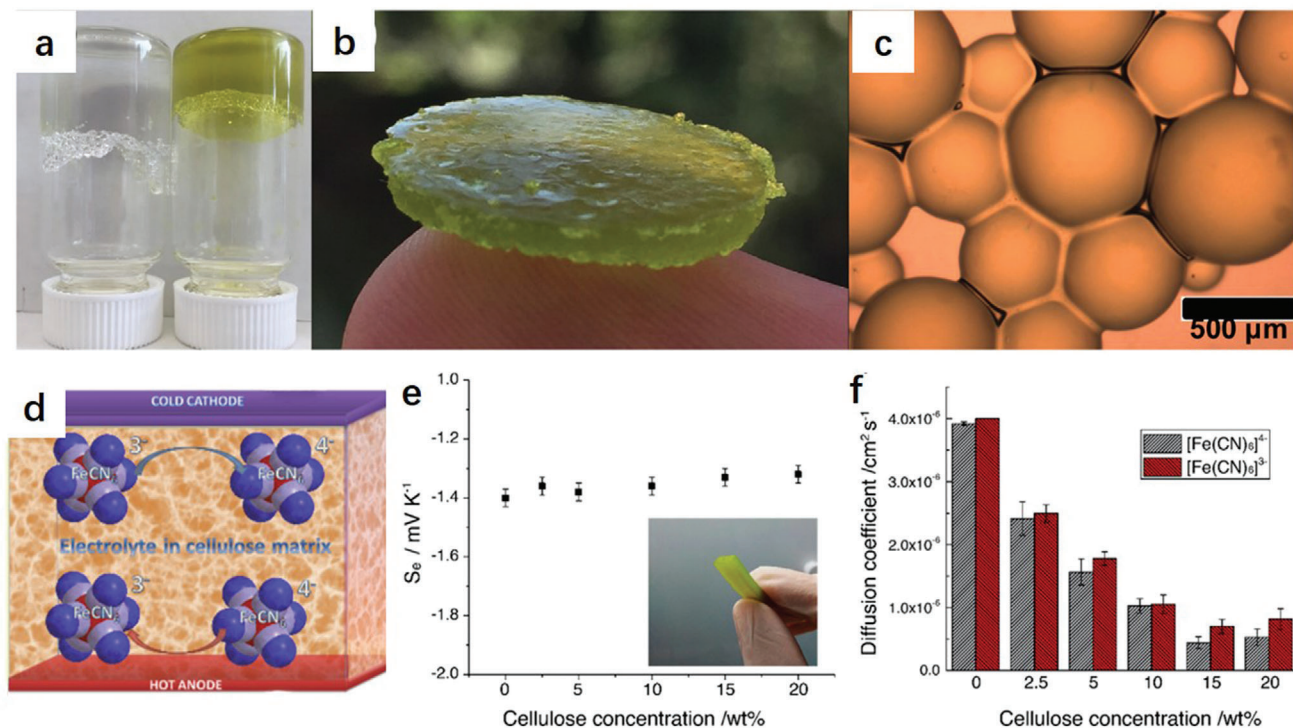


Figure 5. Displaying photographs of a) gels prepared with 5.5 wt% poly(sodium acrylate) with just water (transparent) and with 0.1 M $K_3[Fe(CN)_6]/0.1$ M $K_4[Fe(CN)_6]$ (yellow), passing the inversion test, and b) freestanding gel on a fingertip prepared with 5.5 wt% agar agar and 0.1 M $K_3[Fe(CN)_6]/0.1$ M $K_4[Fe(CN)_6]$, cut to size for the CR2032 internal cavity. Also shown is c) an optical microscope image of a thin layer of a typical 5.5 wt% poly(sodium acrylate) gel. a-c) Reproduced with permission.^[89] Copyright 2016, Elsevier. d) Illustration of the biphasic cellulose- $K_{3/4}FeCN_6$ gel electrolytes. e) Seebeck coefficients of the aqueous solution and the solidified electrolytes (error bars are based on the largest observed standard deviation for the different systems); the inset shows the physical appearance of the solid redox electrolyte with 5 wt% cellulose. f) Diffusion coefficients of $[Fe(CN)_6]^{4-}$ and $[Fe(CN)_6]^{3-}$ in the solution and the solid electrolytes at 22 °C. d-f) Reproduced with permission.^[90] Copyright 2016, American Chemical Society.

and the container is turned upside down. A gel will not flow under its weight as it possesses a higher storage modulus (G') than loss modulus (G''), while the liquid (even a viscous liquid) will show significant flow.

Similarly, Pringle et al. also verified a series of polymers, among which the polyanionic carboxymethylcellulose sodium (CMC) and polyacrylamide (PAAm) were shown to be the most effective hosts for $K_{3/4}Fe(CN)_6$ based electrolyte in terms of thermal energy harvesting.^[91] In this study, gel electrolytes based on other polymers including polyurethanes (HydroMed D₆₄₀ and HydroSlip) and PVA were also employed but were not regarded as a suitable host for $K_{3/4}Fe(CN)_6$. The former gels accommodated 0.4 M $K_{3/4}Fe(CN)_6$ but showed very low Seebeck coefficients and power output (<0.005 mW m⁻²), while the latter one encountered serious flocculation problems when the redox concentration of $Fe(CN)_6^{3/4-}$ was above 0.05 M, resulting in limited power output (0.005 mW m⁻² K⁻²). Both the CMC- $K_{3/4}FeCN_6$ gels and PAAm- $K_{3/4}FeCN_6$ contains a high concentration of redox species (0.4 M) and could achieve both a high Seebeck coefficient (-1.25 and -1.43 mV K⁻¹) and maximum power outputs (0.029 and 0.027 mW m⁻² K⁻²).

It should be noted that the PAAm gel electrolyte developed in this work is a chemically cross-linked and free-standing gel electrolyte. It is mechanically stronger than the abovementioned gel electrolytes which are cross-linked physically by hydrogen bonding, hydrophobic interactions, or electrostatic interactions. While

those gels are flow and leakage free, they cannot maintain their original shape with applied deformation or heating. The robust mechanical properties of the PAAm gel electrolyte enable the thickness to be minimized to 1 mm without encountering of electronic short-circuits between two electrodes during the deformation of the TGC device. The thinner electrolyte decreases the ion diffusion pathway and further enhances the performance of PAAm gel electrolytes from 0.027 mW m⁻² K⁻² (thickness = 10 mm) to 0.071 mW m⁻² K⁻² (thickness = 1 mm).

Another promising gel electrolyte is developed by incorporating the $K_{3/4}Fe(CN)_6$ electrolyte into a well-developed cellulose matrix via a solvent exchange method (Figure 5d,e).^[90] In contrast to other gel electrolytes described above, it is a biphasic quasi-solid-state electrolyte as opposed to a gel, as the polymer of cellulose is insoluble in water. In this quasi-solid-state electrolyte, the cellulose formed a porous network which could lock in the 0.4 M $K_{3/4}Fe(CN)_6$ aqueous electrolyte, and also provide mechanical properties from a “soft sponge” to a “tough rubber” with the concentration of cellulose ranging from 2.5 to 20 wt%. Meanwhile, the addition of the cellulose network also plays an important role in the thermal energy harvesting of $K_{3/4}Fe(CN)_6$ species due to the additional heat transfer pathway and tortuous ion diffusion channel provided by the high 3D and honeycomb-like porous structure of the cellulose network. After optimization, the electrolyte with 5 wt% cellulose content exhibited the highest Seebeck coefficient value of -1.38 mV K⁻¹ and power density of

14 mW m⁻² at $\Delta T = 15$ K (0.062 mW m⁻² K⁻²) at a distance of 3 mm between two nickel electrodes.

It can be observed that the performance of gel electrolytes is highly inferior to the liquid counterparts in terms of power output due to the low ion transport/diffusion rate. To overcome this problem, efforts are focused on the incorporation of additives in the electrolyte/electrode surface or into the gel electrolyte. The addition of gold nanoparticles on the surface between a graphite electrode and a sodium polyacrylate gel electrolyte could lower the electron transfer resistance on the surface and lead to a 20% increase of output power, whereas such improvement is offset by long-term stability issues as the inert gold nanoparticle is unstable in the presence of K_{3/4}FeCN₆ under thermogalvanic conditions.^[92] In addition, ionic liquids (ILs) are also incorporated to improve the electrochemical reversibility of the redox reactions, however, ILs reduce the ion diffusion coefficient with the increased viscosity.^[91] Future work will focus on alternative IL candidates that can increase the solubility of redox couples and lower the viscosities of ILs.

To conclude, significant progress has been made on gel-based p-type electrolytes through a screening selection of compatible polymers, optimization on the polymer content, and the thickness of gel electrolytes, enabling the successful fabrication of gel electrolytes working in TCCs. While these gels remain inferior to their liquid counterparts, great progress has been made.

Gel Electrolytes Consisting of n-Type Redox Couples of Co(bpy)₃^{2+/3+}, Fe^{2+/3+}, I⁻/I₃⁻: Apart from the most extensively investigated p-type redox of Fe(CN)₆^{3-/4-}, various n-type redox couples including Co(bpy)₃^{2+/3+}, Fe^{2+/3+}, I⁻/I₃⁻ were also incorporated into various polymers to achieve comparable performance with p-type gel electrolytes.

[Co(bpy)₃][NTf₂]_{2/3} (where bpy = 2,2'-bipyridyl and NTf₂ = bis(trifluoromethanesulfonyl)amide) has a large and positive Seebeck coefficient of 1.5–2.2 mV K⁻¹ in organic solvents due to the additional entropy effects arising from the spin-state change of the central metal ion (Co^{2+/3+}) during the redox reaction.^[59]

Based on this redox couple, Pringle et al. investigated two kinds of quasi-solid-state electrolytes. First, they use polyvinylidene difluoride (PVDF) and poly(vinylidene fluoride-co-hexafluoropene) (PVDF-HFP) as gelator and prepared the gel electrolyte via the mixing and gelation method (Figure 6a).^[93] The prepared PVDF-based electrolytes show superior performance in terms of a higher temperature range of gel states (<70 °C vs < 60 °C), higher diffusion coefficient, and lower mass-transfer resistance due to the impeded ion diffusion raised by the interactions between the [Co(bpy)₃]³⁺ cations and the polar groups on the PVDF-HFP polymer. With the similar S_e of both gels at around 1.80–1.84 mV K⁻¹, PVDF-based gels containing 0.05 M [Co(bpy)₃][NTf₂]_{2/3} shows a higher power density of 6 mW m⁻² than 4.5 mW m⁻² in PVDF-HFP gels at the same ΔT of 40 °C. Subsequently, the PVDF-based gels were further optimized via tuning the polymer content, the concentration of redox couples and electrode separation. The results show that the P_{max}/ ΔT^2 could be improved from 0.00375 to 0.014 mW m⁻² K⁻² with 5 wt% PVDF, 0.1 M redox couple and an electrode separation of 1 mm. It should be noted here that PVDF-HFP is a highly piezoelectric polymer,^[95,96] and ordered gels formed from these polymers could complement the charge generated by the TGC, in the studies here no deformation was applied to the device and

thus the reported values are from thermo-electrochemical performance only. Another gel of biphasic cellulose-[Co(bpy)₃][NTf₂]_{2/3} electrolyte is prepared by the solvent exchange method (Figure 6a). Compared with the PVDF-based gel, it is free-standing, robust, and mechanically flexible. After the optimization of polymer concentration, electrolyte thickness, and concentration of redox couple, the gel also can deliver a similar P_{max}/ ΔT^2 of ≈ 0.014 mW m⁻² K⁻².

In consideration of the toxic and flammable nature of organic solvents, the environmentally friendly aqueous-based gel electrolytes are more desirable for wearable applications. A cellulose-[Co(bpy)₃]_{2/3} water-based gel electrolyte was therefore developed.^[68] Due to the changed solvent environment and unknown mechanism, the Seebeck coefficient decreased greatly from +1.83 to 1.15 mV K⁻¹. The current density and power output are further limited by the low maximum concentration of [Co(bpy)₃]_{2/3} (0.05 M) in water, with a relatively low P_{max}/ ΔT^2 of only 0.003 mW m⁻² K⁻². Water-based Co(bpy)₃^{2+/3+} gels electrolyte need further study, and the investigations of gels based on alternative n-type redox couples are required.

The cationic Fe^{2+/3+} is one of the well-developed redox couples, which is soluble at high concentrations and has good chemical stability in water with S_e varying from 0.5 to 1.76 mV K⁻¹ depending on the counter anions (e.g., Cl⁻, SO₄²⁻, NO₃⁻, ClO₄⁻).^[67] Particularly relevant is the strong acidic nature of the Fe^{2+/3+} in water due to hydrolysis effects, which complements the required gelation environment for PVA.^[97]

Zhou et al. directly mixed PVA and FeCl_{2/3} solutions and produced a PVA-FeCl_{2/3} film through a mold. The gel film exhibits superior stretchable properties with a strain up to 500% of its original length. Despite the gel exhibiting a much higher thermal conductivity of 1.88 W m⁻¹ K⁻¹ than the liquid counterpart (0.6 W m⁻¹ K⁻¹), it has less heat convection through the polymer matrix, while the Seebeck coefficient is maintained at 1.02 mV K⁻¹ which is close to the value of aqueous electrolytes (≈ 1 mV K⁻¹). Meanwhile, the gel electrolyte has an electrical conductivity comparable to solid-state electrolytes at around 10 mS cm⁻¹, and could deliver a constant normalized current density of 0.13 A m⁻² K⁻¹ and normalized power density of 0.033 mW m⁻² K⁻², which is higher than the Cobalt-based redox couples in an organic gel system.^[88]

Another PVA-FeCl_{2/3} gel electrolyte was prepared by an in situ chemical crosslinking method (Figure 6b) and delivered comparable performance (0.85 mV K⁻¹ and 0.033 mW m⁻² K⁻² in long-term power delivering test).^[82] It should be noted that with the chemical crosslinking of polymer chains via glutaraldehyde (GA), the gel electrolyte exhibits not only flexibility, stretchability and also excellent elastic properties, with only 10% plastic deformation after repeated cyclic stretching to 100% strain for 60 cycles. The gel could also recover its shape after repeated bending and twisting, which increases the potential of this gel electrolyte in wearable applications and even epidermal devices.

The power output of PVA-FeCl_{2/3} gel electrolyte is catching up to that of K_{3/4}Fe(CN)₆ based gel electrolytes. Recently, a perchlorate electrolyte of Fe(ClO₄)_{2/3} was explored for TGCs, exhibiting both a higher Seebeck coefficient of 1.76 mV K⁻¹ and current density than the K_{3/4}Fe(CN)₆ liquid electrolyte.^[67] It is reasonable to believe that the Fe(ClO₄)_{2/3}-based gels will be developed

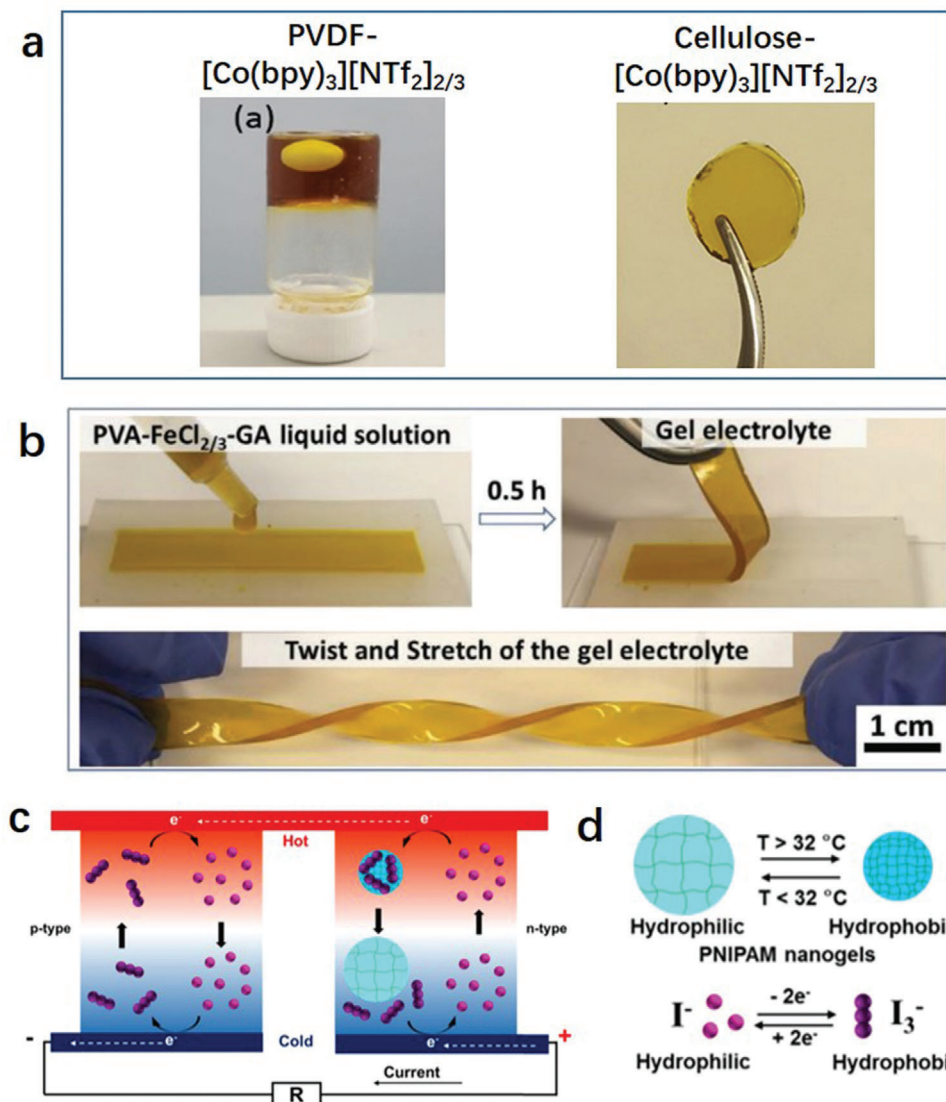


Figure 6. a) Photo of PVDF-[Co(bpy)₃][NTf₂]_{2/3} and cellulose-[Co(bpy)₃][NTf₂]_{2/3} gel electrolytes. left: Reproduced with permission.^[93] Copyright 2018, Wiley-VCH. right: Reproduced with permission.^[68] Copyright 2018, Elsevier. b) Illustration of the preparation of the PVA-FeCl_{2/3} gel electrolyte. Reproduced with permission.^[82] Copyright 2020, Wiley-VCH c) Schematic of the p-n conversion mechanism for the I⁻/I₃⁻ system. d) The hydrophilic/hydrophobic conversion of PNIPAM nanogels and the equilibrium reaction between I⁻ and I₃⁻. c,d) Reproduced with permission.^[94] Copyright 2019, Elsevier.

in the near future, which could be comparable to the p-type gel electrolytes.

I⁻/I₃⁻ is a redox couple with an intrinsically positive Seebeck coefficient, whereas Zhou et al. have prepared a gel electrolyte with converted high negative Seebeck coefficient utilizing a thermosensitive polymer of poly (*N*-isopropylacrylamide) (PNIPAM) (Figure 6c,d).^[94] The PNIPAM nanogels synthesized by emulsion polymerization have a transition temperature at ≈32 °C, above which the gel transforms from a hydrophilic to a hydrophobic state. In these PNIPAM nanogels, the relatively hydrophobic I₃⁻ can be captured by the dehydrated nanogels at the hot side through the hydrophobic interaction and released at the cold side, yielding a concentration gradient of free I₃⁻ across the cell and resulting in the inversion of the Seebeck coefficient from 0.71

to -1.91 mV K⁻¹. Benefiting from a higher value of the absolute Seebeck coefficient, the prepared PNIPAM-I⁻/I₃⁻ gel electrolyte delivers a maximum power output of 0.35 μW that is seven times higher than the pristine I⁻/I₃⁻ aqueous electrolyte. This work opens a new perspective for controlling the Seebeck coefficient of redox couples in gel electrolytes. Besides, the transition temperature of 32 °C matches well with the temperature of the human body, making it specifically suitable for body heat harvesting.

A comparison between the discussed gels is provided below in Table 1. Of note, there is a strong matching in Seebeck coefficient and power output for the CMC-Fe(CN)₆^{3-/4-} p-type gel and the PVA-Fe^{2+/3+} n-type gel, indicating this couple could provide a strong starting point for studying alternating p-n device geometries, which will be discussed further in the following section.

Table 1. Comparison of discussed gel electrolytes for wearable TGC devices, orange colored cells correspond to p-type, and blue to n-type electrolytes.

Redox species	Concentration of redox species	Matrix	Seebeck coefficient [mV K ⁻¹]	Power output [mW m ⁻² K ⁻²]	Comments	Refs.
Fe(CN) ₆ ^{3-/4-}	0.02 M	PVA	-1.21	0.012	First report of gel electrolytes for TGCs	[88]
Fe(CN) ₆ ^{3-/4-}	0.1 M	Poly(sodium acrylate)	-1.09		Highly reversible redox chemistry, excellent diffusion	[89]
Fe(CN) ₆ ^{3-/4-}	0.4 M	CMC	-1.25	0.029	High concentration of redox species	[91]
Fe(CN) ₆ ^{3-/4-}	0.4 M	PAAm	-1.43	0.071	High concentration of redox species; Chemically cross-linked and freestanding electrolyte	[91]
FeCN ₆ ^{3-/4-}	0.4 M	Cellulose	-1.38	0.062	Is a biphasic quasi-solid-state electrolyte rather than a true gel	[90]
[Co(bpy) ₃][NTf ₂] _{2/3}	0.1 M	PVDF	1.8	0.014	Achieved 1 mm thickness	[93]
[Co(bpy) ₃][NTf ₂] _{2/3}	0.1 M	Cellulose		0.014	Is a biphasic quasi-solid state electrolyte rather than a true gel	[68]
Co(bpy) ₃]Cl _{2/3}	0.05 M	Cellulose	1.15	0.003	Is a biphasic quasi-solid-state electrolyte rather than a true gel	[68]
FeCl _{2/3}	1 M	PVA	1.02	0.033	Freestanding and stretchable electrolyte	[88]
FeCl _{2/3}	1 M	PVA	0.85	0.033	Crosslinked via glutaraldehyde, excellent elastic properties	[82]
I ⁻ /I ₃ ⁻		PNIPAM	-1.91		Inverted polarity of the redox couple	[94]

2.3. Potential Design Strategies for Wearable Thermogalvanic Cells

The fabrication of a flexible device requires that all parts of the device are flexible, while maintaining a high performance of thermal energy harvesting. Apart from the flexible electrodes and gel electrolytes, the packaging materials and/or the substrate of electrode materials are usually flexible polyethylene terephthalate (PET) or polyimide sheets, and the electric connections are usually copper wires, sputter-coated gold or platinum.^[79] Currently, all the single-cell devices are constructed in a sandwich structure for the shortest ion pathway and high-power output.

Kim et al. fabricated a flexible device using the CNT-ACT electrodes.^[75] The device was constructed using a conventional sandwich structure, where flexible PET sheets and fabric were employed as packaging materials and separators, respectively. After sealing the device by hot pressing, an aqueous electrolyte of 0.4 M K_{3/4}FeCN₆ was injected to obtain an intact, flexible, TGCs device. The fabricated devices are pliable to accommodate curved shapes including the body and pipes with various curvatures. When attached to a shirt worn by a person and connected to a

capacitor, the TGCs device could harvest body heat, charge the capacitor to 1.2 mV in 10 s and achieve a maximum output power density of 0.46 mW m⁻². This work provides us a typical model in developing a flexible TGCs device concerning all components, despite that the low voltage output from this single device is far from the needs of wearable electronics.

To continue to develop flexible TGCs for implementation into real-world wearable applications, the electrically series connection of single cells is necessary to multiply the voltage output. The arrangement of p-type and n-type devices alternately connected in series is an emerging state-of-art strategy, which avoids the hot-to-cold thermal short-circuit between adjacent cells occurring in devices with the same polarity.^[60] Meanwhile, it should be noted that a comparable output current between p-type and n-type devices is necessary for the efficient series connection, which should be achieved via the optimization of both electrolytes and electrodes for both p-type and n-type devices.

Zhou et al. provided demonstrations of flexible TGCs made by multiple p-n cells for body heat harvesting.^[88,94] In this work, polyimide was used as the substrate for the patterned Au electrodes and electrical interconnections, with the gel

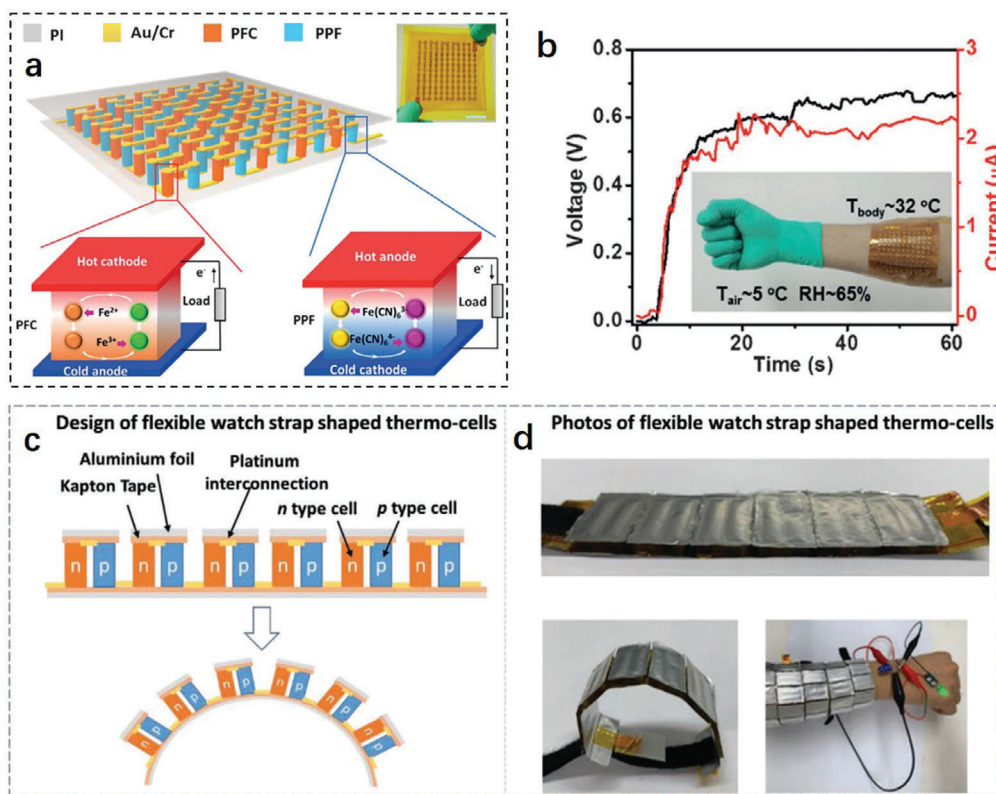


Figure 7. a) The integrated gel-based thermocell. Both the PFC and PPF gels were sandwiched between two flexible substrates (polyimide, PI). With alternating top and bottom interconnections, the PFC and PPF gels are connected sequentially in series. The magnified insets illustrate the operation mechanism of the gel-based thermocell. At a certain temperature difference, the thermovoltage polarity of PFC and PPF is exactly reversed. The top right inset is a photograph of the integrated device (scale bar: 2 cm). b) The voltage and current generated by the thermocell from body heat. The inset shows a photograph of the wearable thermocell on a hand. a, b) Reproduced with permission.^[88] Copyright 2016, Wiley-VCH. c) Schematic and d) photos of the flexible watch-strap shaped p–n thermocell for body-heat harvesting. c, d) Reproduced with permission.^[82] Copyright 2020, Wiley-VCH.

electrolyte placed in the designated location (Figure 7a). An elastic polyurethane frame with a number of holes for individual cells was used when a liquid electrolyte was involved. The work demonstrated that the flexible TGCs consisting of more than 50 pairs of p-type and n-type devices (p–n cells) could generate an output voltage above 0.6 V (Figure 7b) and charge capacitors with a capacitance of 100 μF when worn on the arm of a person. Chen et al. also made multiple pair of p–n cells, where the PEDOT/PSS-based composite film was optimized according to the selected gel electrolytes and boosted the transient power output. 18 pairs of p–n cells could achieve a voltage output of more than 300 mV, charge electrochemical supercapacitors with capacitance as large as 470 mF, and power the light-emitting diodes (LED) lights at a small ΔT of 10 °C. Meanwhile, to maintain uniform heat transfer through electrodes and make it comfortable to wear, strategies including the use of thermally conductive aluminum foil and the design of top-electrodes separated between adjacent pair of p–n cells were employed. The device consisting of 30 pairs of p–n cells worn on the arm of a person could charge 470 mF supercapacitors and power a green LED with a voltage booster during long-term wear (Figure 7c, d).

3. Potential Wearable Thermally Charged Capacitors

3.1. Thermally Charged Capacitors

Thermally charged capacitors (TCCs) (also called thermally charged supercapacitors, ionic thermoelectric supercapacitors, or ionic thermoelectric capacitors) is the combination of a thermal harvester and an energy storage reservoir. TCCs also consists of two electrodes connected by an ionic conductive electrolyte, in which the electrolyte generates thermovoltage and the capacitive electrode store the generated energy (Figure 8).^[40,47]

The thermovoltage is raised from the distinct mobility of cations and anions in the electrolyte under a temperature gradient due to the Soret effect.^[98] The resulting gradient of ion concentration induces the potential difference between two electrodes and the charge induced by the potential difference at the electrode/electrolyte can then be stored by capacitive electrode materials.^[40,47]

As the power output is not constant in TCCs, the energy storage is an important parameter in addition to the figure-of-merit

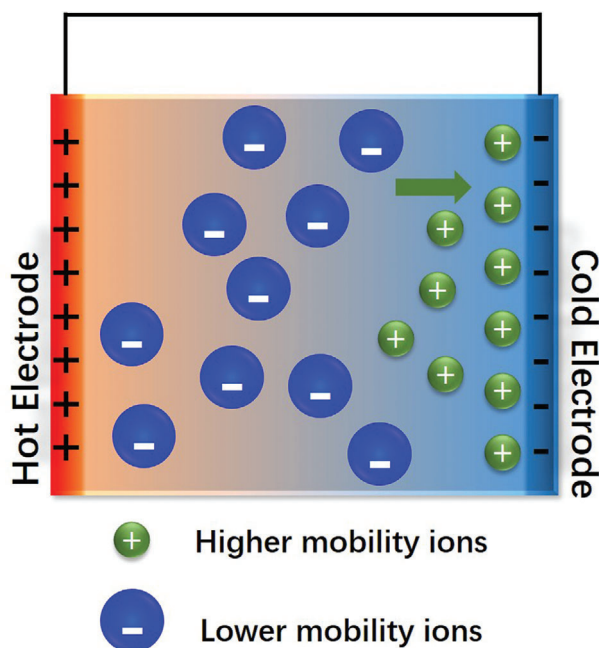


Figure 8. Schematic illustration of a TCC device.

(ZT value) of ionic conductive electrolytes. Energy storage in an idea TCC could be simply defined as:

$$E_{\text{ch}} = \frac{1}{2} \frac{Q_{\text{ch}}^2}{C} = \frac{1}{2} CV^2 \quad (3)$$

where E_{ch} is the charged energy on the electrode, Q_{ch} is the charge stored on the electrode materials, C is the capacitance of the electrode materials in the ionic conducting electrolyte, V is the thermovoltage. Therefore, both capacitances of the electrode materials, as well as the thermovoltage produced by ionic conducting electrolytes are of vital importance to achieve the high performance of a TCCs.^[99]

Meanwhile, the thermal conductivity and ionic conductivity of the electrolytes also play a role in the effective utilization of thermal energy and electric energy, so the ionic figure-of-merit (ZT_i) can also be applied here to evaluate the performance of ionic conductive electrolytes as below:

$$ZT_i = S_i^2 \sigma T / \kappa \quad (4)$$

where S_i is ionic seebeck coefficient, σ is the ionic conductivity, T is the absolute temperature and κ is the thermal conductivity.^[40,47]

To achieve high thermoelectrochemical performance and advance the wearable application of TCCs, efforts have been focused on developing flexible electrode materials, solid-state and flexible electrolytes, as well as an optimization of the device design.

3.2. Potential Materials for Wearable Thermally Charged Capacitors

3.2.1. Flexible Electrode Materials

The role of electrode materials in the TCCs is to store the charge (or energy) accumulated on the electrode/electrolyte interface generated by TCCs electrolytes, so capacitive materials including metal plates, carbon materials, and conducting polymers are used. Based on the energy storage mechanism, electrode materials can be classified into electrical double layer capacitive (EDLC) and pseudocapacitive materials.^[100] EDLC electrodes physically store the separated charge on the surface, so an electrically conductive and chemically inert material with a large ion-accessible surface area like porous carbon materials usually shows higher capacitance than chemically inert metal plates. Pseudocapacitive materials, like conducting polymers and metal oxides, store energy via the reversible faradic reactions between the ions and electrodes and can provide much higher capacitance than EDLCs. Flexible electrode materials using both the EDLCs and pseudocapacitive mechanism have been extensively studied in the area of flexible supercapacitors, some of which are chosen and utilized in TCCs based on the composition of the electrolytes.^[45,100–102]

Crispin et al. prepared a thick CNT film on sputter-coated gold film via a drop-casting method.^[101] Due to the high effective surface area of the nanoporous CNT network ($\approx 120\text{--}430 \text{ m}^2 \text{ g}^{-1}$), the CNT–Au electrode exhibits a larger EDLCs capacitance of 1.03 mF cm^{-2} than the pure gold electrode of $5.1 \text{ }\mu\text{F cm}^{-2}$ in a PEO–NaOH polymer electrolyte and can store the energy of $1.35 \text{ }\mu\text{J cm}^{-2}$ at a $\Delta T = 4.5 \text{ K}$ (Figure 9a–c). This indicates the effectiveness of introducing nano-porous electrodes in TCCs devices.

Apart from carbon materials, conducting polymers with large pseudocapacitance were used in proton-based electrolytes, which will be electrically oxidized (doped) and reduced (de-doped) in acidic environments when there is a potential difference (Figure 9d,e).^[102] Wang et al. synthesized a novel flexible conjugated conducting polymer of PDAQ-BC via the Buchwald-Hartwig coupling method between 2,6-diaminoanthraquinone (DAQ) and 3,6-dibromo-9-(4-bromophenyl)carbazole (DBC) with nanoparticle morphologies (diameter of 100 nm). The nanostructured PDAQ-BC has a large surface area of $358 \text{ m}^2 \text{ g}^{-1}$ and the anthraquinone moieties exhibit excellent redox properties, so this flexible PDAQ-BC-based electrode produced a pseudocapacitance of 102 mF cm^{-2} in the TCCs using PSSH film as an electrolyte.

Composite materials combining the EDLC and pseudocapacitive materials were also prepared to achieve an enhanced capacitance.^[45] Yu et al. deposited pseudocapacitive polyaniline (PANi) on nanoporous graphene/nanotube (G/CNT) films via an electropolymerization method. The prepared PANi@G/CNT electrode exhibited three to seven times higher capacitance (410 F g^{-1}) than the G/CNT electrode (150 F g^{-1}) and pure CNT electrodes (52 F g^{-1}) in $1 \text{ M H}_2\text{SO}_4$ due to the large surface area of the carbon materials and the high redox activity of PANi. When assembled into TCCs, the PANi@G/CNT produced an extremely high capacitance of 487 mF cm^{-2} in PSSH solid electrolyte, which is the highest value among all the TCCs devices. Due to the large capacitance, the device can store energy up to 0.173 mJ cm^{-2} at a temperature gradient of 5.3 K (thermovoltage was 38 mV).

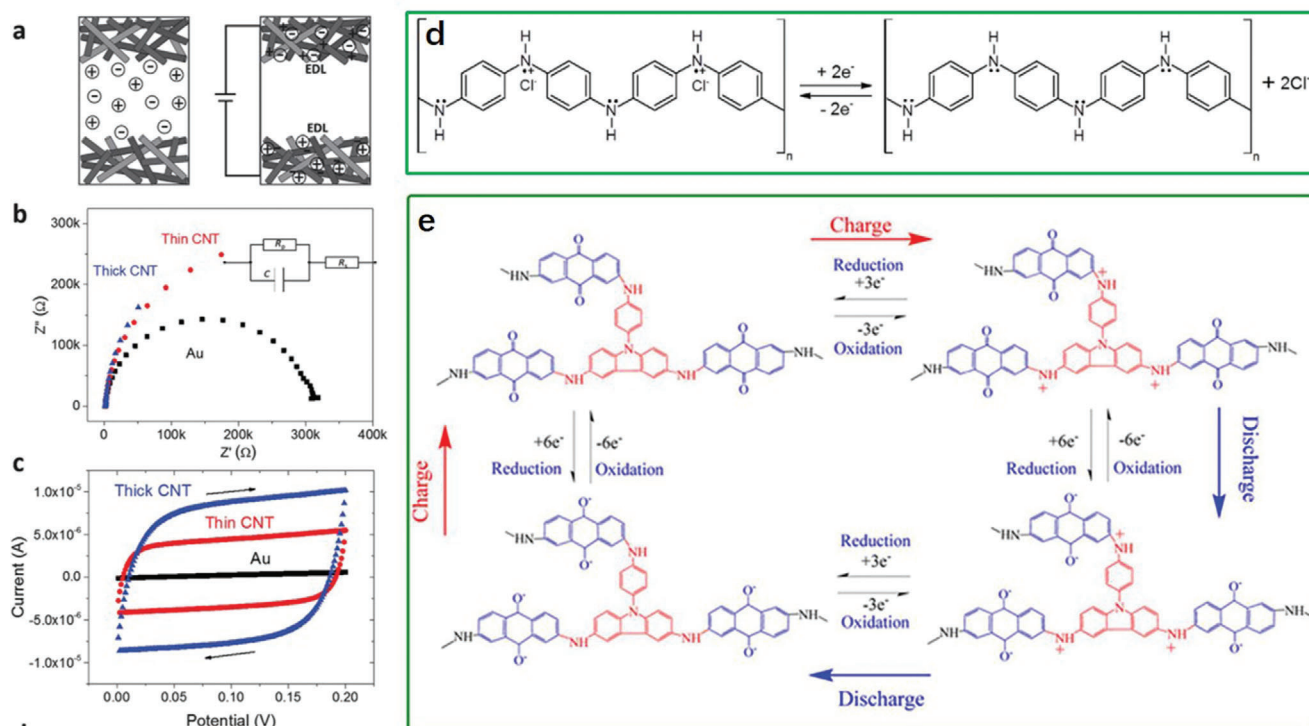


Figure 9. a–c) Capacitance properties of NaOH–PEO with the CNT electrode. a) Illustration of the electric double layer (EDL) formed in CNT electrodes.^[101] Copyright 2016, The Royal Society of Chemistry. b) Nyquist plots for devices with Au, thin CNT, and thick CNT electrodes in the frequency range of 100 kHz to 1 MHz. The inset shows the simulated equivalent circuit: R_p : resistance connected parallel to the capacitance that is associated with the leakage current; R_s : resistance connected series which represents the internal resistance of the device; C: the capacitance. c) CV curves of devices with the three different types of electrodes, measured at 10 mV s^{-1} . a–c) Reproduced with permission.^[101] Copyright 2016, The Royal Society of Chemistry. d) Redox reactions of PANI during the charging and discharging processes. PANI switches between emeraldine salt and leucoemeraldine base by accepting and releasing electrons during the reduction and oxidation process, respectively. Reproduced with permission.^[45] Copyright 2016, Wiley-VCH. e) Charge–discharge mechanism for PDAQ-BC. Reproduced with permission.^[102] Copyright 2019, Elsevier.

However, there are only a few investigations on high-performance flexible electrode materials for TCCs, which is probably because the emergence of ionically conductive electrolytes for TCCs is still in its infancy. More focus on developing electrode materials will be paid after the electrolyte is extensively studied and developed, and the abundance of supercapacitor literature can be used as a starting point for matching the electrodes with the electrolytes once they are developed.

Solid-State Electrolytes: Most of the electrolytes utilized in TCCs are usually viscous or solid-state polymer electrolytes^[45,46,103] and viscous ionic liquids,^[104] so there is almost no leakage consideration for wearable utilization. To achieve a more comfortable experience for users and to increase the endurance of the device under repeated deformations during usage, efforts have been paid to endow the electrolytes with superior mechanical properties including flexibility, stretchability, and even self-healing properties.

Polyanions with Sulfonic Groups: In most polymer electrolytes for TCCs, those consisting of small cations and anionic polymer chains with sulfonic groups on the side chains such as PSSH,^[45] polystyrene sulfonate sodium (PSSNa),^[46] and poly(2-acrylamido-2-methyl-1-propanesulfonic acid) (PAAMPSA)^[103] have attracted the most attention. Due to the huge mobility difference of the lighter proton or sodium ions, and the heavy poly-

mer anion along the temperature gradient, large ionic thermopotentials are produced with ionic Seebeck coefficients of 8, 3, and 5.6 mV K^{-1} for PSSH, PSSNa, and PAAMPSA, respectively, in a humid environment, which is much higher than the TGC and TEG devices.

However, the fragile and brittle nature of these polymer electrolytes will undoubtedly limit the application in flexible electronics, and thus additives should be incorporated to improve the mechanical properties.^[46] Crispin et al. incorporated commonly used flexible additives of cellulose (nanofibrillated cellulose, NFC) into the polyelectrolyte of PSSNa. The prepared NFC–PSSNa solid-state electrolyte is mechanically robust, flexible, and foldable compared to PSSNa (Figure 10a,b), exhibits a high value of tensile strength ($\sigma_T = 16.6 \pm 1.5 \text{ MPa}$), calculated Young's modulus of $E = 0.9 \pm 0.1 \text{ GPa}$ and a strain at break of $\epsilon_T = 10.2 \pm 1.2\%$, which is sufficient for practical handling and processing in roll-to-roll machines. Despite the relatively lower ionic conductivity (0.004 S m^{-1}) of the composite NFC–PSSNa compared to that of the pure PSSNa electrolyte (0.026 S m^{-1}) at the low humidity of 50% RH, the values increased to a similar level at high humidity of 100% RH with 0.9 S m^{-1} and 12 S m^{-1} for NFC–PSSNa and PSSNa, respectively. Meanwhile, the existence of NFC has increased the ionic Seebeck coefficient from 3 to 8.4 mV K^{-1} at 100% RH, which is probably due to the entanglement of the

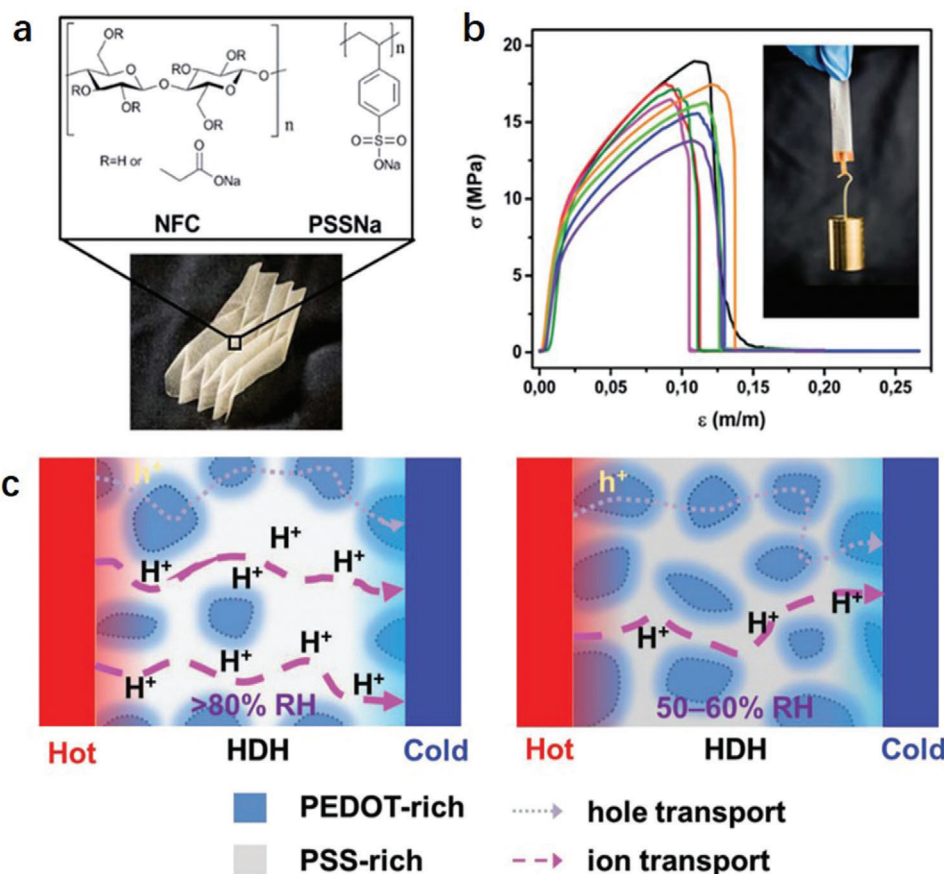


Figure 10. a) Photograph of flexible NFC–PSSNa paper as well as the chemical structure of nanofibrillated cellulose (NFC) and polystyrene sulfonate sodium (PSSNa). b) Tensile strength versus strain for eight different NFC–PSSNa samples with the same composition and thickness. Inset is the photograph of an 80 mm thick NFC–PSSNa strip subjected to a weight of 100 g. The photographs were taken by Thor Balkhed (Linköping University). Reproduced with permission.^[46] Copyright 2017, The Royal Society of Chemistry. c) Schematic images of carrier transfer such as electronic and ionic carriers in the HDH film at different RH. Reproduced with permission.^[105] Copyright 2018, Wiley-VCH.

immobile PSS^- by the nanofibers of cellulose. As a result, the composite NFC–PSSNa can achieve an overall figure-of-merit (0.025) higher than the PSSNa alone (0.006), indicating the success in pursuing both improved mechanical and thermoelectric chemical performance.

Compared to the insulating additives, an electrically conductive and mechanically flexible polymer of PEDOT:PSS can achieve a further enhancement of the thermoelectrochemical performance of PSSH-based electrolyte.^[105] PEDOT:PSS is a commercialized conducting polymer with a core–shell structure, in which the core of PEDOT is an electronic thermoelectric material exhibiting an electric Seebeck coefficient of $\approx 200 \mu\text{V K}^{-1}$ and the PSS shell is the polymer electrolyte wrapped PEDOT with negative charges and π - π stacking. Kim et al. found that by varying the weight ratio of PEDOT:PSS to 1:9 via the doping of purchased PEDOT:PSS by PSSH, the composite electrolyte is a mixed ionic–electric conductor (Figure 10c) and can produce a high ionic Seebeck coefficient of 16.2 mV K^{-1} , the ultrahigh ionic conductivity of 29.1 S m^{-1} , and a high-power factor of $7.6 \text{ mW m}^{-1} \text{ K}^{-2}$ at 90% RH humidity. This arises from the fast proton mobility through the ionic conduction channels created inside

the composite polymer film and the trap of PSS^- by negatively charged PEDOT.

In addition to flexibility, stretchability and self-healing properties are also highly relevant for wearable applications. Those properties can allow larger deformations of TCC devices without degrading the electronic performance and restore the mechanical integrity and thermoelectrochemical performance when damage does occur under deformation. For this purpose, Jang et al prepared a ternary composite electrolyte material, in which the conjugated polymer of polyaniline (PANI) and a physical cross-linker of phytic acid (PA) was added into proton conductive anionic polyelectrolyte of PAAMPSA. The PANi:PAAMPSA:PA ternary film exhibited excellent stretchability to 750% strain and self-healable property without any external stimuli in a relative moisture environment (Figure 11).^[103] The excellent mechanical properties are caused by the synergetic contribution from the dynamic hydrogen bonding in PANi/PA and PAAMPSA/PA and electrostatic interactions between PANi and PAAMPSA (Figure 11a). In addition, the additional protons from the PO_3H_2 group of PA also improved the protonation in the sulfonic acid of PAAMPSA

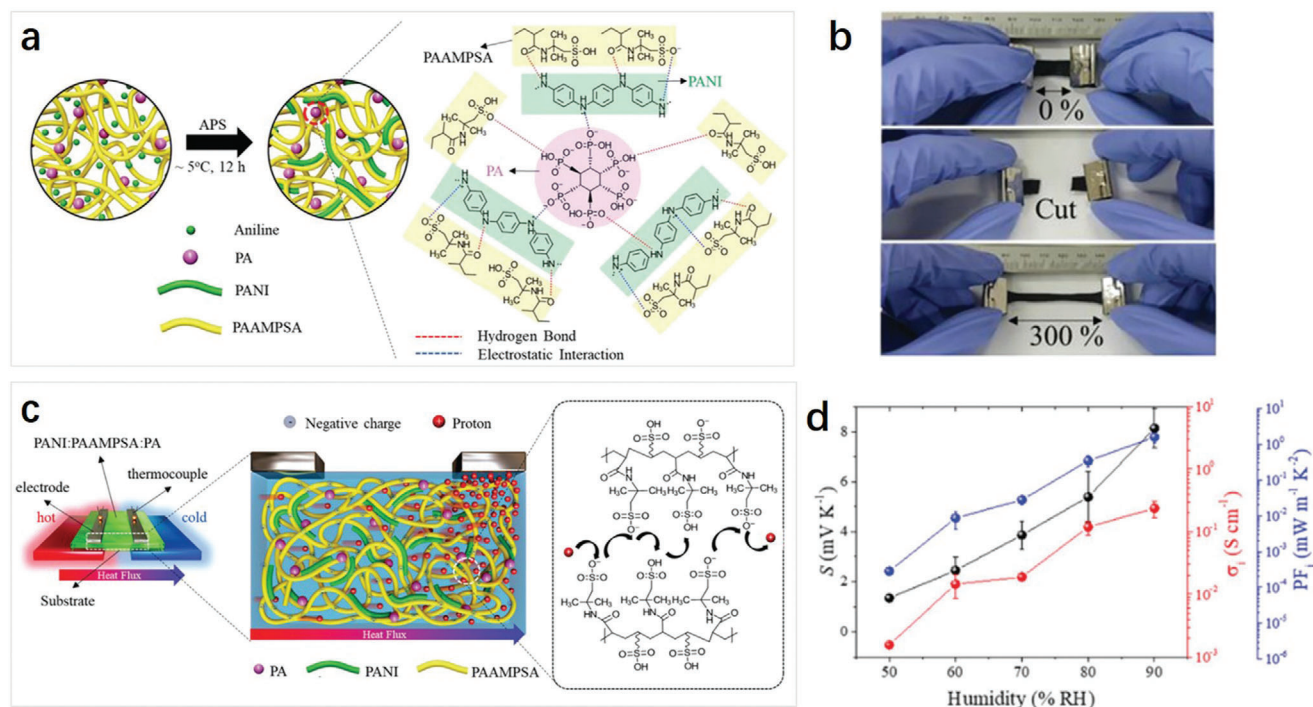


Figure 11. a) Schematic illustration and molecular structures of PANI:PAAMPSA:PA ternary TE hybrids. The crosslinking forms regenerative dynamic networks through hydrogen bonds and electrostatic interactions between PANI, PAAMPSA, and PA. b) Photograph of a TE hybrid film during the self-healing and stretching test. c) Schematic illustration of the proton diffusion in a PANI:PAAMPSA:PA ternary hybrid film under a temperature difference. d) Seebeck coefficient, ionic conductivity, and ionic power factor of the TE hybrid at different humidity levels. The point values and error bars indicate the average and standard deviation respectively. Reproduced with permission.^[103] Copyright 2020, The Royal Society of Chemistry.

and enhanced proton transport, so the film electrolytes exhibited an ultra-high ionic conductivity of 25.6 S m⁻¹ (Figure 11c,d). Meanwhile, the polymer chains with sulfonic acid groups were more immobile due to the chain entanglement and the physical crosslinking with PA and PANi, so the ionic Seebeck coefficient increased from 5.6 mV K⁻¹ for pure PAAMPSA conductors to 8.1 mV K⁻¹ in the ternary composite at 90% RH humidity. As a result of the synergetic enhancement of the three components on the ionic conductivity, Seebeck coefficient, and mechanical properties, the composite film exhibits a high figure-of-merit of 1.0 without performance degradation under 50% strain and after the cut-healing process.

It can be conceived that sulfonic polyanion-based electrolytes could be mechanically robust, and exhibit a huge ionic Seebeck coefficient compared to TEG and TGCs. Meanwhile, the high capacitance of pseudocapacitive conducting polymers for the proton conductive sulfonic polyanion electrolytes could further enhance the thermo-electrochemical performance of TCCs.

Ionic Liquid-Based Electrolyte: Ionic liquids (ILs) are regarded as promising liquid electrolytes for thermally charged capacitors due to their relatively high ionic conductivity and boiling points, low thermal conductivity (<0.61 W m⁻¹ K⁻¹) as well as negligible vapor pressure.^[41,47] The remarkable feature of ILs is that the ions cannot pass into an external circuit when diffusing to the electrode surface. Hence, the diffusion of ions under a temperature difference usually generates a high thermovoltage between electrodes. These properties imply that the ILs are expected to improve the output power and heat-to-electricity conversion ef-

iciency of TCCs. However, wearable devices require the TCCs have excellent mechanical properties and enough safety performance, while the pure ILs are difficult to meet such requirements due to their poor mechanical properties and possible leakage. Furthermore, the ionic Seebeck coefficient of the pure ILs is very small (such as [EMIM][TFSI], the ionic Seebeck coefficient only has -0.85 mV K⁻¹)^[104] due to the small difference in diffusion coefficients between their anions and cations. Generally, a larger difference in diffusion coefficients between anions and cations can lead to larger S_{td} values.

The thermodiffusion difference highly depends on the interactions between ions and polymer matrix. When ILs are mixed with fluorinated polymers (such as PVDF-HFP), a small fraction of anions tend to condense along the negatively charged polymer chains due to the strong electron-withdrawing character of the F-groups (Figure 12a). These condensed anions near the polymer chains could increase the frictional drags of cations, thus reducing their mobility, while the rest of anions that are not condensed around the polymer chains can remain highly mobile, or vice versa. Therefore, ILs can integrate with flexible polymers to enlarge the differences of their constituent ion diffusion coefficients, and then achieve high-performance wearable TCCs.

Polymer electrolyte matrices, such as poly(vinylidene fluoride-co-hexafluoropropylene) (PVDF-HFP),^[106,107] polyurethane (WPU),^[108] and SiO₂ nanoparticle^[109] are considered as promising solid carriers for liquid ILs. For instance, when 40 wt% 1-ethyl-3-methylimidazolium dicyanamide ([EMIM][DCA], an IL) was mixed with WPU ([EMIM][DCA]/WPU) through a

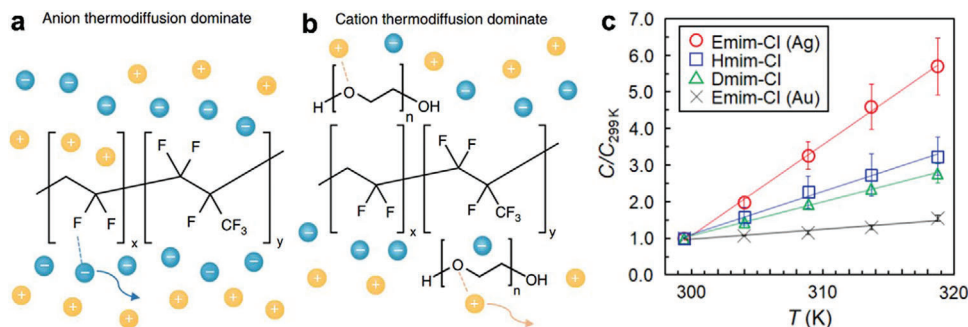


Figure 12. Engineering strategies for the negative or positive tuning of S_{id} . a) Anions tend to condensate along negatively polymer chains due to the strong electron-withdrawing character of the F-groups. b) PEG (PEG interacts preferentially with cations) along the polymer chains hinder the PVDF/anion interaction, thereby promoting thermodiffusion of cations rather than anions. a, b) Reproduced with permission.^[104] Copyright 2019, Springer Nature. c) The interfacial polarizability caused by the difference of interaction strength between the cations/anions and electrode depends on the type of metal electrode material. Reproduced with permission.^[110] Copyright 2020, American Chemical Society.

so-called “drop casting the aqueous solutions” process, the prepared polymer ionogel electrolytes show a high Seebeck coefficient of 34.5 mV K^{-1} (relative humidity of 90%) and possess remarkable mechanical robustness with the mechanical stretchability of up to 156%.^[108] Such an enhanced positive sign of the Seebeck coefficient is mainly attributed to the thermodiffusion of anions in the polymer ionogels being strongly limited by the polar groups of WPU, thus the cations thermodiffuse more easily than the anions. In contrast to these IL/polymer electrolytes, the SiO_2 nanoparticles also show excellent properties in tuning the ionic conductivity and ionic Seebeck coefficient. Since the hydroxy groups on SiO_2 nanoparticles tend to attract the anions thus causing the SiO_2 surface to be negatively charged. Such electrostatic interactions between the negatively charged anions and polar hydroxy groups are usually regarded as ion-dipole interactions, which can disrupt the short-range ordered structure of ionic liquids, thereby creating channels for ion transport and decreasing the activation energy of the ionogels. Based on this mechanism, the ionic conductivity and Seebeck coefficient of [EMIM][DCA] can be greatly enhanced to 14.8 mV K^{-1} and $4.75 \times 10^{-2} \text{ S cm}^{-1}$ after 20 wt% SiO_2 nanoparticles (20 nm) are added in [EMIM][DCA].^[109] It is noted that the thermoelectric properties of polymer ionogels are proportional to the ambient humidity and IL loading. For example, when the relative humidity increases from 30% to 90%, the S_{id} of [EMIM][DCA]/WPU ionogels significantly increases from 8.3 to 34.5 mV K^{-1} .^[108]

Furthermore, we can conveniently tune the type (p or n-type) of polymer ionogel electrolytes by virtue of the dependence of their ions thermodiffusion on the polarity of the polymer matrix. Such a strategy is conducive to integrate p- and n-type thermocells to generate sufficient output voltage and power for real-world wearable applications. Fluorinated polymer ionogels [EMIM][TFSI]/PVDF-HFP usually exhibit a negative Seebeck coefficient. However, once the [EMIM][TFSI]/PVDF-HFP ionogels are doped by the liquid polyethylene glycol (PEG), the measured S_{id} can be changed from -4 to $+14 \text{ mV K}^{-1}$.^[104] This occurs due to the presence of PEG along the polymer chains which can hinder the PVDF/anion interaction while the PEG interacts preferentially with cations, such changes ultimately promote thermodiffusion of [EMIM] cations rather than [TFSI] anions (Figure 12b).

On the other hand, different ILs usually exhibit different ionic adsorption and desorption behaviors on the surface of metal electrodes with increasing ambient temperature. Accordingly, a potential difference will be generated between metal electrodes under a temperature gradient. This approach also can be used to integrate p- and n-type thermoelectric unit arrays by choosing different types of IL.^[111] Importantly, the thermo-voltage of TCCs exhibits a significant dependence on the metal electrode material (Au, Ag) due to the difference in interfacial polarizability caused by the difference of interaction strength between the cations/anions and electrode materials (Figure 12c).^[110]

Other Electrolytes: In addition to these mainstream polyanion- and IL-based electrolytes, the redox couples, and aqueous polymer-inorganic electrolyte mixtures (such as polyethylene oxide (PEO)-NaOH) also can be employed to integrate with the flexible matrix material. The $[\text{Fe}(\text{CN})_6]^{3-}/[\text{Fe}(\text{CN})_6]^{4-}$ redox couple is commonly used as an electrolyte in TGCs, which can be used as an additive to electrolytes (such as PVA- $\text{K}_3\text{Fe}(\text{CN})_6/\text{K}_4\text{Fe}(\text{CN})_6$) in thermally charged capacitors and works as the electrolytes in TCCs.^[112,113] The thermovoltage is also generated from the thermal-dependent redox reactions occurred on the wet electrolyte/electrode interface. The PVA matrix in the totally dried PVA- $\text{K}_3\text{Fe}(\text{CN})_6/\text{K}_4\text{Fe}(\text{CN})_6$ electrolyte layer hinders the migration of redox ions and the charge is therefore stored on the electrolyte/electrode interface. PEO-NaOH is a typical aqueous polymer-inorganic electrolyte mixture, when NaOH was added to liquid PEO, the terminating alcohol groups (-C-OH) would be transformed into anionic alkoxide end groups (-C-O-Na⁺), while the rest of Na⁺ that has not condensed around the polymer chains can retain its mobility.^[101] Particularly, the Seebeck coefficients of PEO-NaOH electrolytes can be significantly increased from 10 to 24 mV K^{-1} if such electrolyte is infiltrated into the well-aligned and negatively charged cellulose II.^[114] Since the thermovoltage or Seebeck coefficients of thermally charged capacitors strongly depend on the mobility difference between the anion and cation ions of electrolytes. The negatively charged cellulose II would combine with the Na⁺ to form the Na-cellulose complex, which could increase frictional drags of anions while promoting the mobility of cations. Nevertheless, even if the polymer ionogel electrolytes

Table 2. Summary of the typical electrolyte for TCCs.

Electrolyte	S_e [mV K ⁻¹]	σ [S m ⁻¹]	κ [W m ⁻¹ K ⁻¹]	Power factor [mW m ⁻¹ K ⁻²]	ZT factor ^{a)}	Comments	Refs.
PEO–NaOH	11.1	0.00813	0.216	0.001	0.00127	Polycation-based electrolyte	[101]
PSSH	8	9	0.38	0.576	0.414	The first sulfuric polyanion-based solid electrolytes	[45]
NFC–PSSNa	8.4	0.9	0.75	0.0635	0.0231	Flexible, robust, and soft	[46]
PEDOT:PSS/PSSH	16.2	29.1	0.11	7.637	20.3	Flexible and has a high ZT value	[105]
PANI:PAAMPSA:PA	8.1	25.6	0.451	1.679	1.09	Stretchable and self-healable electrolyte	[103]
[EMIM][TFSI]/PVDFHFP/PEG	14	0.6	0.136	0.117	0.236	The sign and value of S_e can be tuned.	[104]
[EMIM][DCA]/PVDF-HFP/PEDOT:PSS	–4	0.6	0.136	0.00960	0.0193	The hybrid ionic and electronic thermoelectric converter	[107]
WPU/EMIM:DCA Ionogels	34.5	0.84	0.23	1.00	1.27	stretchable and transparent electrolyte	[108]
[EMIm][TFSI] n type	2.6	0.877	/	0.00593	/	p-n in series connection design on cellulose paper	[111]
[EMIm][Ac] p-type	2.2	0.334	/	0.00162	/		
PVA-Rmim-Cl	10	0.116	0.2	0.0116	0.0170	Ionic hydrogels	[110]
PEO–NaOH-Oxidized cellulosic membrane	24	2	0.48	1.1520	0.655	Well-aligned and porous polymer matrix	[114]
PVA-K _{3/4} Fe(CN) ₆	1.21	1	1.85	0.00146	0.000216	The use of thermogalvanic gel electrolyte	[113]

Note: ^{a)}The ZT factor is calculated at a $T = 293$ K if the value is not given in the ref.

can retard water evaporation, the intrinsic aqueous feature still makes them inevitably suffer from water loss through vaporization even under ambient conditions, which is adverse to their long-term application.

A comparison between the typical TCCs electrolyte is provided in **Table 2**. The ionic Seebeck coefficient and ionic conductivity are highly dependent on not only the nature of cation and anions but also on the chemical nature and the structure of polymer matrix. Meanwhile, it has to be noted that all the high-performance values are achieved at very high humidity and decrease rapidly when RH% is gradually reduced (**Figure 13**), which greatly limits the application where TCCs are suitable. The reason for this humidity dependent on the performance of sulfonic polyanionic-based electrolyte is clarified by Kim et al and provided examples to overcome the limitation in the application environment.^[105] The decrease in performance with decreasing humidity occurs as the dissociation of Na⁺ and protons only occurred in media with high water content, and the ionic conduction channels also rely on the swell of hygroscopic PSS-rich domains. To overcome this problem, Kim et al. developed a self-humidifying layer consisting of a water-absorbing MOF layer and hydrogel water supplying layer was utilized to keep the humidity of the TCCs devices high, which provide a new perspective to broaden the application environment of TCCs.^[105]

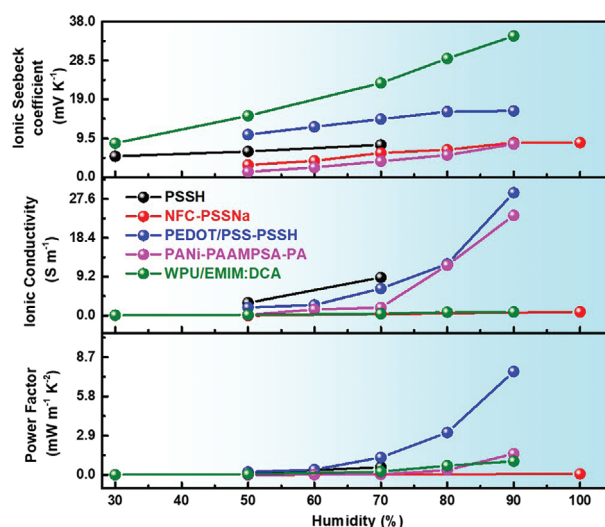


Figure 13. Humidity dependence of performance merits (i.e. ionic Seebeck coefficient, ionic conductivity, and power factor) for several typical TCCs electrolytes. Data of the drawn samples are obtained from references as below: PSSH from ref.[45], NFC-PSSNa from ref.[46], PEDOT/PSS-PSSH from ref.[105], PANi-PAAMPSA-PA from ref.[103], and WPU/EMIM:DCA from ref.[108].

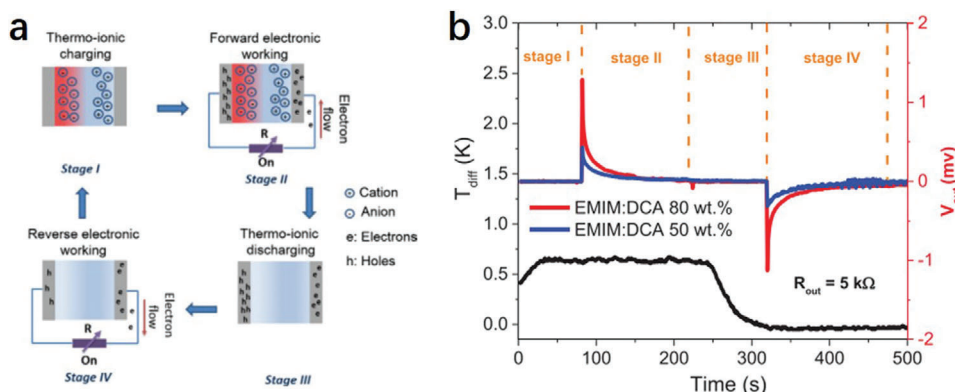


Figure 14. a) Illustration of the working principles of ionic thermoelectric capacitors. b) Voltage profiles of the external load connected with ionic thermoelectric capacitors using EMIM:DCA/PVDF-HFP ionogels with 50% and 80 wt% IL loadings and silver electrodes. Reproduced with permission.^[106] Copyright 2019, Wiley-VCH.

3.3. Potential Design Strategies for Wearable Thermally Charged Capacitors

In addition to the sandwiched construction common in TGCs, TCC devices can also be designed in a planar structure that is much more thinner and flexible.^[105] Meanwhile, the working mode of TCCs is also different. Unlike continuous power delivery at a constant ΔT in TGCs, TCCs work in a discontinuous manner and require human intervention to realize the storage of thermally generated electric energy.^[106]

In brief, TCCs work in four steps (Figure 14).^[106] At stage I, thermovoltage is generated by the accumulation of ions and the counter ions on hot and cold electrodes respectively under the temperature difference. At stage II, the external load was connected to the TCCs, where the electrons transport through the external circuit to balance the charge of ions on the electrode/electrolyte interface. Then at stage III, the ions and counter ions accumulated on the electrodes will retract in the absence of temperature gradient and the electrical charge stored on electrode materials will be maintained under an open circuit state. Lastly, in stage IV, the stored energy can be used to power an external load in the absence of a temperature gradient. Thus, for body-heat harvesting and powering wearable electronics, the TCCs device will be finally used in the absence of temperature gradient (i.e., taken off or heat isolated from the human skin). Specifically, the device has to be externally connected to a load when worn on the skin and then disconnected without a temperature gradient for use. This process is tedious for users and requires further designs on the electric circuit to simplify the usage process.

In addition, the series connection of single TCCs is also required to increase output voltage for real applications. The state-of-the-art p–n series connection is also applied for the effective utilization of heat (Figure 15a), where the electrode and electrolyte were coated or printed one-by-one on the designed location of the flexible substrate (paper or PET).^[111] Due to the apparent larger ionic Seebeck coefficient of TCC than that of TGCs, a large voltage of 30 mV and 1.65 V can be generated by single devices and 20 TCCs, when heated by a fingertip (Figure 15b) and at a small temperature difference of 5 K (Figure 15c), respectively.^[105] The results show the great advantage and potential application of TCCs. However, the tedious four-step working

mode impeded the application of TCCs in energy storage and powering electronics, more work on the device and electric circuit designs should be paid.

4. Other Type of Wearable Electrochemical Cells

High heat-to-electricity conversion efficiency is conducive to increase the output energy of thermocells, which in turn reduces the number of cell integrations for wearable sensors. Hence, we can power one or even more wearable sensors with one thermocell rather than dozens or even hundreds of thermocells. However, the commercial viability of thermocells is now severely limited by their rather low heat-to-electricity conversion efficiency (typically below 1%).^[39] To address such problems, researchers have designed a direct thermal charging cell (DTCC) that is different from the traditional thermogalvanic and thermodiffusion strategies.^[115] The charging operation of DTCCs can be directly finished by isothermal heating without the need for external electricity and temperature gradient. When the DTCCs are cooled down at room temperature, the system can be self-regenerated. Therefore, DTCCs require a fluctuant temperature environment to function, being applicable to intermittent heat sources (such as solar energy).

A DTCC containing $\text{Fe}^{2+}/\text{Fe}^{3+}$ redox electrolyte connected to asymmetric electrodes of a graphene oxide/platinum nanoparticles (GO/PtNPs) cathode and a polyaniline (PANI) anode, which can store the generated thermo-voltage through the temperature-induced pseudocapacitive effect of GO and the thermogalvanic effect of $\text{Fe}^{2+}/\text{Fe}^{3+}$ redox couples was fabricated (Figure 16a).^[115] The intrinsic low boiling point of the aqueous electrolyte and thermal charging mechanism limits the operating temperature of DTCCs in the range of 40–90 °C. Importantly, this DTCC device achieves excellent performance with a high α of up to 5.0 mV K^{-1} and η up to $\approx 3.52\%$ at 90 °C.^[115] For DTCCs, it is important to protect the functional groups of GO from being reduced as the C=O and O=C=O functional groups in the GO play a key role in the thermal-charging mechanism. This requires a redox couple with a positive temperature coefficient ($\alpha > 0$, such as $\text{Fe}^{2+}/\text{Fe}^{3+}$, I^-/I_3^- , Cu/Cu^{2+}) so that heating facilitates the reduction reaction at GO/PtNPs cathode instead of the oxidation reaction ($\alpha < 0$, such as $\text{Fe}(\text{CN})_6^{4-}/\text{Fe}(\text{CN})_6^{3-}$). The reduction reaction process of

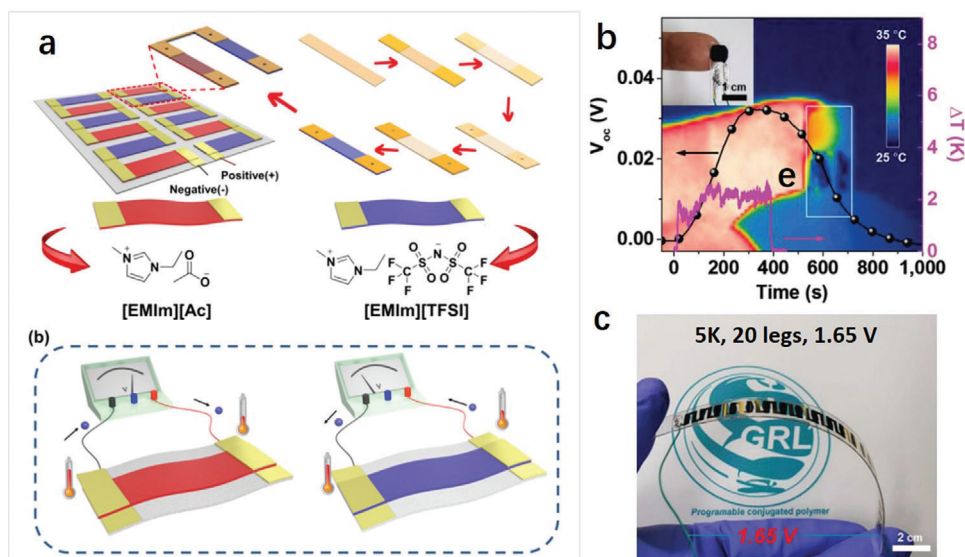


Figure 15. a) Typical fabrication process of the single thermoelectric unit and thermoelectric module based on the connection of [EMIm][Ac] (p-type) and [EMIm][TFSI] (n-type) thermoelectric units in series, and Schematic diagram of thermoelectric voltages of [EMIm][Ac]- or [EMIm][TFSI]-based thermoelectric units in the case of a temperature difference between two electrodes.^[111] Copyright 2020, American Chemistry Society. b) A direct thermal capacitor that charged upon contact to a fingertip as a heat source. Inset: A photo image and IR camera image of the HDH30 with contact of the fingertip. Reproduced with permission.^[111] Copyright 2020, American Chemistry Society. c) A photo image of a module-type flexible PMIC with 20 legs. Reproduced with permission.^[105] Copyright 2019, Wiley-VCH.

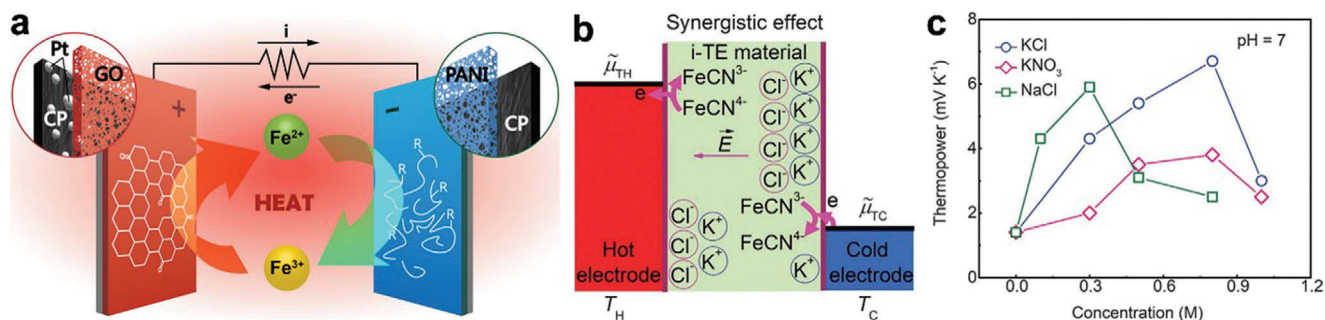


Figure 16. New engineering strategies for wearable thermocells. a) $\text{Fe}^{2+}/\text{Fe}^{3+}$ redox electrolyte connected to asymmetric electrodes. Reproduced with permission.^[115] Copyright 2019, Springer Nature. b) synergistic thermodiffusion and thermogalvanic effects. c) Thermopower of gelatin-KCl, gelatin- KNO_3 , and gelatin-NaCl with varying electrolyte concentrations. b, c) Reproduced with permission.^[116] Copyright 2020, The American Association for the Advancement of Science.

redox couples can consume most electrons from the oxidation of PANI anode through the external circuit. Particularly, the preferential reduction reaction of redox couples at GO/PtNPs cathode also can greatly increase the potential difference between asymmetric electrodes. However, such cells remain an ongoing challenge for continuous operation before avoiding the consumption problem of PANI anodes.^[117]

Thermo-electrochemical cells (thermocells) offer a promising and inexpensive strategy for harvesting body heat in a room temperature environment. However, the output voltage and power of current thermocells are insufficient to support the normal operation of commercial wearable sensors. Recently, another advanced synergistic strategy by combining thermodiffusion and thermogalvanic effects to increase the total thermopower S_i provides a feasible direction to address current challenges (Figure 16b).^[116] Such a strategy needs to combine a redox couple with a negative

temperature coefficient ($\alpha < 0$) and ion providers with p-type thermodiffusive thermopower ($S_{\text{td}} > 0$), or vice versa. The goal is to ensure that the direction of the inner electric field produced by the thermodiffusion of ion providers is consistent with the shifting direction of the electrochemical potential of the thermogalvanic effect.

Based on this synergistic strategy, the flexible thermocells with S_i up to 17 mV K^{-1} have been obtained in a gelatin matrix modulated with 0.8 M KCl for thermodiffusion effect and $0.42/0.25 \text{ M Fe(CN)}_6^{4-/3-}$ redox couple for thermogalvanic effect.^[116] Importantly, this novel thermocells works in a quasicontinuous mode, thus it can be used repetitively rather than being a one-time energy source. Given the significant difference of mass diffusion coefficient of different cations and anions in the water channel of gelatin matrix, and most of the thermopower contribution comes from the thermodiffusion effect of ion providers (the

Table 3. The comparison between wearable TGCs and TCCs.

	Wearable TGCs	Wearable TCCs
Mechanism	Thermogalvanic effect: continuous conversion from heat to electricity	Thermodiffusion effect: Storage of the electric energy converted from heat
Electrode	Electrically conductive materials with high catalytic behavior	Electrically conductive materials with high capacitance
Electrolyte	Electrolytes containing redox couples	Electrolytes with different size of cation and anion.
Seebeck coefficient	In the range of 0.5–2 mV K ⁻¹	Up to 34.5 mV K ⁻¹
Device architecture	Sandwiched structure	Sandwiched or planar structure
Working modes	Continuous operation without the need of manual interfere	Manual mode in four steps
Working requirements	/	High humidity
Cost	Low cost	TCCs with ionic liquids-based electrolyte is expensive

relative contribution over 60%), thus the selection of ion providers is critical for the final attainable S_e . Among the ion providers, KCl demonstrates maximum thermopower than KNO₃ and NaCl (Figure 16c). When 25 of such thermoelectric elements are connected in series using copper electrodes, the output voltage and power are up to 2.2 V and 5 μ W ($\Delta T \cong 10$ K), respectively.^[116] These performance indexes can be matched with many commercial sensors. Hence, such a synergistic strategy shows great application potential in body heat harvesting for powering wearable sensors.

5. Conclusion, Challenges, and Perspective

To conclude, we have summarized the recent development of potentially wearable TECs of both TGCs and TCCs in this review and made comparisons between TGCs and TCCs in Table 3. It can be found that both potentially wearable TGCs and TCCs have been developed in the past several years and progress was achieved in terms of the flexible, solid-state electrolytes and device design. The large Seebeck coefficient, low-cost materials, and ease of fabrication make them promising for low-grade body heat harvesting. However, the investigations in both wearable TGCs and TCCs are still in the infant stage especially in the relatively low current output, power output, and heat to electricity conversion efficiency areas. We propose below some future directions which should be studied to achieve higher thermoelectrochemical performance and practical application.

5.1. Electrode Materials

Flexible or stretchable materials with well-defined and tunable porosity, high electrical and thermal conductivity are desired in pursuing high-performance TEC devices. These properties ensure a high ion accessible surface area, unobstructed ion diffusion channel, and good electron and thermal transfer. Nanostructured carbon materials (like graphene and carbon nanotubes), PEDOT/PSS, and their composites are good candidates and have been extensively developed. The specific design of the porosity (including the size, density, uniformity, and morphology of pores) based on the nature of the conductive ion is necessary. In addition, recently reported stretchable materials made from carbon nanotube or PEDOT/PSS, makes it possible to prepare a

stretchable TECs electrode in the near future.^[3,118] Fibers based on these materials are also encouraged which can exhibit flexibility, conductivity and high surface area once knitted to form textiles.^[119–121]

Rigid bulk materials with high catalytic or capacitive behaviors, like platinum, copper, nickel, metal oxides, polypyrrole, and polyaniline, which have been proved to achieve superior performance in TECs remain unsuitable for wearable and flexible applications.^[69,122] However, with a nanoscale engineering of their morphology by including nanoparticles, nanosheets, or nanowires, they could be incorporated into the flexible, conductive, and porous host materials and have the chance to show their superiority in thermo-electrochemical performance.^[69] Meanwhile, the single-atom dopant of platinum, copper, bimetal is also a good strategy.^[123,124]

5.2. Solid-State Electrolytes

The ionic conductivity of both TGC and TCC solid-state electrolyte is limited in comparison with their liquid counterparts as well as the conventional thermoelectric materials. Strategies that can boost the mobility of ions and create ion diffusion channels should be applied to the polymer host. Thus, the thermo-electrochemical power output and figure of merits will be greatly enhanced for TGC and TCCs, respectively.

The Seebeck coefficient of the TGC gel electrolytes can be further enhanced. Recently, additives like chaotropic cations, amide derivatives, and organic micelles were added in Fe(CN)₆^{3-/4-} to improve the S_e to 4.2 mV K⁻¹.^[63] Different kinds of α -CDs were used which has temperature-dependent host–guest interactions with redox couples, increased the S_e to 2.6 mV K⁻¹.^[66] All these values are higher than that of the gel electrolytes (below 1.8 mV K⁻¹). It is believed these strategies in liquids electrolytes could be extended into the gel system for enhanced voltage output. Despite the large S_e and good-matching with pseudocapacitive electrodes, the dependence of the Seebeck coefficient on the humidity of proton conductive electrolytes has limited their practical application.^[105] Self-humidifying gels are expected to develop in TCCs systems to avoid concerns in the operating environment.^[105]

In addition, the discovery of a new specific mechanism of thermally derived voltage, like the combination of both TGC and TCC electrolytes, the discovery of new redox couples with high reaction entropy change or ion conductive materials with enlarged

mobility difference of anions and cations is urgent to achieve revolutionary progress.

5.3. Device Fabrication

The consideration of thermal management is needed in device fabrication to maximum the actual temperature difference between the two electrodes. The use of an adhesive and curved conformable thin-film substrate for electrodes near the skin side, like polydimethylsiloxane (PDMS) and polyurethane (PU) could ensure the intimate contact between skin and the device for effective heat transfer.^[36] On the sides exposed to the air, it is possible to involve some flexible heatsink, examples of which include a thin layer of superabsorbent cross-linked polymers that can cool the device by water evaporation.^[125]

The series connection between the n-type and p-type device is still necessary for the application, as the generated voltage of a single device from the temperature difference between skin and the outside environment cannot be meet the needs for wearable electronics. Before designing the p–n connection circuit, the matching of the n-type and p-type device in terms of comparable current output is of great importance to make full use of the electric energy generated by the thermal gradient.

Low-cost technologies in fabricating p–n series circuits and with precisely localized electrodes and electrolytes in p–n cells are also encouraged to promote large-scale fabrication and realize commercialization. 3D printing could enable the formation of the sandwiched structured device with 3D features, tailored to a custom body part.^[126,127] Other printing technologies like inkjet printing, spray coating, screen printing can also be used for the planar structured TCCs device and applied as supplementary techniques in the sandwiched device.^[126,127] However, the investigation on printable ink formulations based on the materials are preconditions of continued development in this area.^[126,127]

5.4. Integration and Applications

There are great differences in the application between TGCs and TCCs devices. The former provides continuous power output under temperature difference, whereas in the latter case a four-step intervention of the user is required to realize the charge storage on electrodes.

TGC devices could directly power some low-power electronics in a continuous way. Alternatively, it could be coupled with energy storage units (like capacitors, batteries, or supercapacitors) which can store the accumulated or the spared energy and drive the electronics with high energy consumption. Additional voltage booster and regulatory circuits should be considered when designing the whole apparatus. In TCCs, after the voltage is raised from the temperature difference, the device has to experience an electrical charge under ΔT , the disconnection of the external circuit without ΔT for ion recovery, and finally connect to the external circuit to power electronics. The process is tedious for users and a humanization design on electrical/thermal switches is required.^[47]

The emerging advances in wireless data communication technologies have greatly decreased the energy demands of wearable

electronics. Some of the health monitoring sensor systems like a cardiogram, movement, or temperature sensing only require tens or hundreds of microwatts, which fits well the power output of wearable TECs and may become the largest application market of wearable TECs.^[33]

In summary, as a newly developed emerging area of research, there are great challenges and also great opportunities for improvements to achieve the application of wearable TECs on body heat harvesting. A bright future towards practical applications and commercialization is anticipated with thorough considerations and a focus on developing electrodes, electrolytes, and devices, while considering their integration.

Acknowledgements

Y.L. and H.W. contributed equally to this work. The authors gratefully acknowledge the support from the National Natural Science Foundation of China (52003037, 52002050, 52002171), China Postdoctoral Science Foundation (2020M673176), the Natural Science Foundation of Jiangsu Province (No. BK20200696, No.20KJB430019), and Australian Research Council (DP170102320 and CE140100012).

Conflict of Interest

The authors declare no conflict of interest.

Keywords

body heat, electrochemical cells, flexible electrodes, solid-state electrolyte, thermal harvesting, wearable electronics

Received: February 17, 2021

Revised: March 22, 2021

Published online: April 29, 2021

- [1] R. Tian, Y. Liu, K. Koumoto, J. Chen, *Joule* **2019**, *3*, 1399.
- [2] S. Zhang, F. Cicoira, *Nature* **2018**, *561*, 466.
- [3] Y. Wang, C. Zhu, R. Pfattner, H. Yan, L. Jin, S. Chen, F. Molina-Lopez, F. Lissel, J. Liu, N. I. Rabiah, Z. Chen, J. W. Chung, C. Linder, M. F. Toney, B. Murmann, Z. Bao, *Sci. Adv.* **2017**, *3*, e1602076.
- [4] Z. Lou, L. Li, L. Wang, G. Shen, *Small* **2017**, *13*, 1701791.
- [5] Q. Shi, B. Dong, T. He, Z. Sun, J. Zhu, Z. Zhang, C. Lee, *InfoMat* **2020**, *2*, 1131.
- [6] S. Xu, Y. Zhang, J. Cho, J. Lee, X. Huang, L. Jia, J. A. Fan, Y. Su, J. Su, H. Zhang, H. Cheng, B. Lu, C. Yu, C. Chuang, T. Il Kim, T. Song, K. Shigeta, S. Kang, C. Dagdeviren, I. Petrov, P. V. Braun, Y. Huang, U. Paik, J. A. Rogers, *Nat. Commun.* **2013**, *4*, 1543.
- [7] W. Song, S. Yoo, G. Song, S. Lee, M. Kong, J. Rim, U. Jeong, S. Park, *Batteries Supercaps* **2019**, *2*, 181.
- [8] Z. Wu, Y. Wang, X. Liu, C. Lv, Y. Li, D. Wei, Z. Liu, *Adv. Mater.* **2019**, *31*, 1800716.
- [9] C. Zhao, Y. Lu, L. Chen, Y. Hu, *InfoMat* **2020**, *2*, 126.
- [10] C. Dai, G. Sun, L. Hu, Y. Xiao, Z. Zhang, L. Qu, *InfoMat* **2020**, *2*, 509.
- [11] Y. Zhao, J. Guo, *InfoMat* **2020**, *2*, 866.
- [12] X. Chen, N. S. Villa, Y. Zhuang, L. Chen, T. Wang, Z. Li, T. Kong, *Adv. Energy Mater.* **2020**, *10*, 1902769.
- [13] Z. Lv, Y. Luo, Y. Tang, J. Wei, Z. Zhu, X. Zhou, W. Li, Y. Zeng, W. Zhang, Y. Zhang, D. Qi, S. Pan, X. J. Loh, X. Chen, *Adv. Mater.* **2018**, *30*, 1704531.

- [14] R. Wang, M. Yao, Z. Niu, *InfoMat* **2020**, 2, 113.
- [15] C. G. Núñez, W. T. Navaraj, E. O. Polat, R. Dahiya, *Adv. Funct. Mater.* **2017**, 27, 1606287.
- [16] D. J. Lipomi, B. C. K. Tee, M. Vosgueritchian, Z. Bao, *Adv. Mater.* **2011**, 23, 1771.
- [17] S. Park, H. Kim, M. Vosgueritchian, S. Cheon, H. Kim, J. H. Koo, T. R. Kim, S. Lee, G. Schwartz, H. Chang, Z. Bao, *Adv. Mater.* **2014**, 26, 7324.
- [18] K. Dong, Z. Wu, J. Deng, A. C. Wang, H. Zou, C. Chen, D. Hu, B. Gu, B. Sun, Z. L. Wang, *Adv. Mater.* **2018**, 30, 1804944.
- [19] M. Chen, X. Li, L. Lin, W. Du, X. Han, J. Zhu, C. Pan, Z. L. Wang, *Adv. Funct. Mater.* **2014**, 24, 5059.
- [20] Y. Liu, L. Wang, L. Zhao, X. Yu, Y. Zi, *InfoMat* **2020**, 2, 318.
- [21] X. Fan, X. Liu, W. Hu, C. Zhong, J. Lu, *InfoMat* **2019**, 1, 130.
- [22] Y. Tang, X. Li, H. Lv, W. Wang, C. Zhi, H. Li, *InfoMat* **2020**, 2, 1109.
- [23] L. Zhao, H. Li, J. Meng, Z. Li, *InfoMat* **2020**, 2, 212.
- [24] S. A. Hashemi, S. Ramakrishna, A. G. Aberle, *Energy Environ. Sci.* **2020**, 13, 685.
- [25] Z. Yang, J. Deng, X. Sun, H. Li, H. Peng, *Adv. Mater.* **2014**, 26, 2643.
- [26] A. Šutka, P. C. Sherrell, N. A. Shepelin, L. Lapčinskis, K. Mālnieks, A. V. Ellis, *Adv. Mater.* **2020**, 32, 2002979.
- [27] D. J. Lacks, T. Shinbrot, *Nat. Rev. Chem.* **2019**, 3, 465.
- [28] B. Kumar, S. W. Kim, *J. Mater. Chem.* **2011**, 21, 18946.
- [29] J. He, T. Wen, S. Qian, Z. Zhang, Z. Tian, J. Zhu, J. Mu, X. Hou, W. Geng, J. Cho, J. Han, X. Chou, C. Xue, *Nano Energy* **2018**, 43, 326.
- [30] M. Tian, D. Zhang, M. Wang, Y. Zhu, C. Chen, Y. Chen, T. Jiang, S. Gao, *Nano Energy* **2020**, 74, 104908.
- [31] C. Zhang, J. Chen, W. Xuan, S. Huang, B. You, W. Li, L. Sun, H. Jin, X. Wang, S. Dong, J. Luo, A. J. Flewitt, Z. L. Wang, *Nat. Commun.* **2020**, 11, 58.
- [32] F. R. Fan, Z. Q. Tian, Z. L. Wang, *Nano Energy* **2012**, 1, 328.
- [33] M. Dargusch, W. Di Liu, Z. G. Chen, *Adv. Sci.* **2020**, 7, 2001362.
- [34] X.-L. Shi, J. Zou, Z.-G. Chen, *Chem. Rev.* **2020**, 120, 7399.
- [35] P. J. Taroni, G. Santagiuliana, K. Wan, P. Calado, M. Qiu, H. Zhang, N. M. Pugno, M. Palma, N. Stingelin-Stutzman, M. Heeney, O. Fenwick, M. Baxendale, E. Bilotti, *Adv. Funct. Mater.* **2018**, 28, 1704285.
- [36] M. Zadan, M. H. Malakooti, C. Majidi, *ACS Appl. Mater. Interfaces* **2020**, 12, 17921.
- [37] Y. Yang, H. Hu, Z. Chen, Z. Wang, L. Jiang, G. Lu, X. Li, R. Chen, J. Jin, H. Kang, H. Chen, S. Lin, S. Xiao, H. Zhao, R. Xiong, J. Shi, Q. Zhou, S. Xu, Y. Chen, *Nano Lett.* **2020**, 20, 4445.
- [38] N. Kim, S. Lienemann, I. Petsagkourakis, D. Alemu Mengistie, S. Kee, T. Ederth, V. Gueskine, P. Leclère, R. Lazzaroni, X. Crispin, K. Tybrandt, *Nat. Commun.* **2020**, 11, 1424.
- [39] Li M., Hong M., Dargusch M., Zou J., Chen Z., *Trends Chem.*, <https://doi.org/10.1016/j.trechm.2020.11.001>.
- [40] X. Wu, N. Gao, H. Jia, Y. Wang, *Chem. - An Asian J.* **2020**, 16, 129.
- [41] M. F. Dupont, D. R. MacFarlane, J. M. Pringle, *Chem. Commun.* **2017**, 53, 6288.
- [42] B. Burrows, *J. Electrochem. Soc.* **1976**, 123, 154.
- [43] Y. Mua, T. I. Quickenden, *J. Electrochem. Soc.* **1996**, 143, 2558.
- [44] T. Ikeshoji, *Bull. Chem. Soc. Jpn.* **1987**, 60, 1505.
- [45] S. L. Kim, H. T. Lin, C. Yu, *Adv. Energy Mater.* **2016**, 6, 1600546.
- [46] F. Jiao, A. Naderi, D. Zhao, J. Schlueter, M. Shahi, J. Sundström, H. Granberg, J. Edberg, U. Ail, J. Brill, T. Lindström, M. Berggren, X. Crispin, *J. Mater. Chem. A* **2017**, 5, 16883.
- [47] A. Al-zubaidi, X. Ji, J. Yu, *Sustain. Energy Fuels* **2017**, 1, 1457.
- [48] F. Zhang, J. Liu, W. Yang, B. E. Logan, *Energy Environ. Sci.* **2015**, 8, 343.
- [49] C. Gao, S. W. Lee, Y. Yang, *ACS Energy Lett.* **2017**, 2, 2326.
- [50] T. I. Quickenden, Y. Mua, *J. Electrochem. Soc.* **1995**, 142, 3985.
- [51] R. Hu, B. A. Cola, N. Haram, J. N. Barisci, S. Lee, S. Stoughton, G. Wallace, C. Too, M. Thomas, A. Gestos, M. E. Dela Cruz, J. P. Ferraris, A. A. Zakhidov, R. H. Baughman, *Nano Lett.* **2010**, 10, 838.
- [52] T. J. Kang, S. Fang, M. E. Kozlov, C. S. Haines, N. Li, Y. H. Kim, Y. Chen, R. H. Baughman, *Adv. Funct. Mater.* **2012**, 22, 477.
- [53] T. J. Abraham, D. R. MacFarlane, R. H. Baughman, L. Jin, N. Li, J. M. Pringle, *Electrochim. Acta* **2013**, 113, 87.
- [54] T. J. Abraham, D. R. MacFarlane, J. M. Pringle, *Chem. Commun.* **2011**, 47, 6260.
- [55] E. Laux, S. Uhl, T. Journot, J. Brossard, L. Jeandupeux, H. Keppner, *J. Electron. Mater.* **2016**, 45, 3383.
- [56] M. A. Buckingham, K. Laws, J. T. Sengel, L. Aldous, *Green Chem.* **2020**, 22, 6062.
- [57] M. A. Buckingham, F. Marken, L. Aldous, *Sustain. Energy Fuels* **2018**, 2, 2717.
- [58] J. T. Hupp, M. J. Weaver, *Inorg. Chem.* **1984**, 23, 3639.
- [59] T. J. Abraham, D. R. MacFarlane, J. M. Pringle, *Energy Environ. Sci.* **2013**, 6, 2639.
- [60] M. Al Maimani, J. J. Black, L. Aldous, *Electrochem. Commun.* **2016**, 72, 181.
- [61] T. I. Quickenden, C. F. Vernon, *Sol. Energy* **1986**, 36, 63.
- [62] T. Kim, J. S. Lee, G. Lee, H. Yoon, J. Yoon, T. J. Kang, Y. H. Kim, *Nano Energy* **2017**, 31, 160.
- [63] J. Duan, G. Feng, B. Yu, J. Li, M. Chen, P. Yang, J. Feng, K. Liu, J. Zhou, *Nat. Commun.* **2018**, 9, 5146.
- [64] H. Inoue, Y. Liang, T. Yamada, N. Kimizuka, *Chem. Commun.* **2020**, 56, 7013.
- [65] Y. Liang, T. Yamada, H. Zhou, N. Kimizuka, *Chem. Sci.* **2019**, 10, 773.
- [66] H. Zhou, T. Yamada, N. Kimizuka, *J. Am. Chem. Soc.* **2016**, 138, 10502.
- [67] J. H. Kim, J. H. Lee, R. R. Palem, M.-S. Suh, H. H. Lee, T. J. Kang, *Sci. Rep.* **2019**, 9, 8706.
- [68] A. Taheri, D. R. MacFarlane, C. Pozo-Gonzalo, J. M. Pringle, *Electrochim. Acta* **2019**, 297, 669.
- [69] H. Im, T. Kim, H. Song, J. Choi, J. S. Park, R. Ovalle-Robles, H. D. Yang, K. D. Kihm, R. H. Baughman, H. H. Lee, T. J. Kang, Y. H. Kim, *Nat. Commun.* **2016**, 7, 10600.
- [70] J. H. Kim, T. J. Kang, *ACS Appl. Mater. Interfaces* **2019**, 11, 28894.
- [71] P. F. Salazar, S. Kumar, B. A. Cola, *J. Electrochem. Soc.* **2012**, 159, B483.
- [72] J. H. Lee, Y. Jung, J. H. Kim, S. J. Yang, T. J. Kang, *Carbon* **2019**, 147, 559.
- [73] K. Wijeratne, M. Vagin, R. Brooke, X. Crispin, *J. Mater. Chem. A* **2017**, 5, 19619.
- [74] L. Hu, M. Pasta, F. L. a Mantia, L. Cui, S. Jeong, H. D. Deshazer, J. W. Choi, S. M. Han, Y. Cui, *Nano Lett.* **2010**, 10, 708.
- [75] H. Im, H. G. Moon, J. S. Lee, I. Y. Chung, T. J. Kang, Y. H. Kim, *Nano Res.* **2014**, 7, 443.
- [76] L. Zhang, T. Kim, N. Li, T. J. Kang, J. Chen, J. M. Pringle, M. Zhang, A. H. Kazim, S. Fang, C. Haines, D. Al-Masri, B. A. Cola, J. M. Razal, J. Di, S. Beirne, D. R. MacFarlane, A. Gonzalez-Martin, S. Mathew, Y. H. Kim, G. Wallace, R. H. Baughman, *Adv. Mater.* **2017**, 29, 1605652.
- [77] Y. Liu, B. Weng, J. M. Razal, Q. Xu, C. Zhao, Y. Hou, S. Seyedin, R. Jalili, G. G. Wallace, J. Chen, *Sci. Rep.* **2015**, 5, 17045.
- [78] M. S. Romano, N. Li, D. Antiohos, J. M. Razal, A. Nattestad, S. Beirne, S. Fang, Y. Chen, R. Jalili, G. G. Wallace, R. Baughman, J. Chen, *Adv. Mater.* **2013**, 25, 6602.
- [79] X. Lu, M. Yu, G. Wang, Y. Tong, Y. Li, *Energy Environ. Sci.* **2014**, 7, 2160.
- [80] Y. Yan, J. Miao, Z. Yang, F. X. Xiao, H. Bin Yang, B. Liu, Y. Yang, *Chem. Soc. Rev.* **2015**, 44, 3295.
- [81] K. Wijeratne, U. Ail, R. Brooke, M. Vagin, X. Liu, M. Fahlman, X. Crispin, *Proc. Natl. Acad. Sci. USA* **2018**, 115, 11899.
- [82] Y. Liu, S. Zhang, Y. Zhou, M. A. Buckingham, L. Aldous, P. C. Sherrell, G. G. Wallace, G. Ryder, S. Faisal, D. L. Officer, S. Beirne, J. Chen, *Adv. Energy Mater.* **2020**, 10, 2002539.

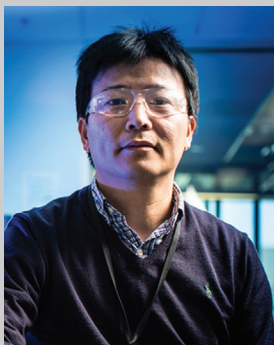
- [83] M. Y. Teo, N. Kim, S. Kee, B. S. Kim, G. Kim, S. Hong, S. Jung, K. Lee, *ACS Appl. Mater. Interfaces* **2017**, *9*, 819.
- [84] J. Ouyang, Q. Xu, C. W. Chu, Y. Yang, G. Li, J. Shinar, *Polymer* **2004**, *45*, 8443.
- [85] X. Crispin, F. L. E. Jakobsson, A. Crispin, P. C. M. Grim, P. Andersson, A. Volodin, C. Van Haesendonck, M. Van Der Auweraer, W. R. Salaneck, M. Berggren, *Chem. Mater.* **2006**, *18*, 4354.
- [86] J. Ouyang, C.-W. Chu, F.-C. Chen, Q. Xu, Y. Yang, *Adv. Funct. Mater.* **2005**, *15*, 203.
- [87] D. Antiohos, G. Folkes, P. Sherrell, S. Ashraf, G. G. Wallace, P. Aitchison, A. T. Harris, J. Chen, A. I. Minett, *J. Mater. Chem.* **2011**, *21*, 15987.
- [88] P. Yang, K. Liu, Q. Chen, X. Mo, Y. Zhou, S. Li, G. Feng, J. Zhou, *Angew. Chem. Int. Ed.* **2016**, *55*, 12050.
- [89] J. Wu, J. J. Black, L. Aldous, *Electrochim. Acta* **2017**, *225*, 482.
- [90] L. Jin, G. W. Greene, D. R. MacFarlane, J. M. Pringle, *ACS Energy Lett.* **2016**, *1*, 654.
- [91] M. Russo, H. Warren, G. M. Spinks, D. R. MacFarlane, J. M. Pringle, *Aust. J. Chem.* **2018**, *72*, 112.
- [92] H. A. H. Alzahrani, M. A. Buckingham, F. Marken, L. Aldous, *Electrochem. Commun.* **2019**, *102*, 41.
- [93] A. Taheri, D. R. MacFarlane, C. Pozo-Gonzalo, J. M. Pringle, *ChemSusChem* **2018**, *11*, 2788.
- [94] J. Duan, B. Yu, K. Liu, J. Li, P. Yang, W. Xie, G. Xue, R. Liu, H. Wang, J. Zhou, *Nano Energy* **2019**, *57*, 473.
- [95] N. A. Shepelin, A. M. Glushenkov, V. C. Lussini, P. J. Fox, G. W. Dincoski, J. G. Shapter, A. V. Ellis, *Energy Environ. Sci.* **2019**, *12*, 1143.
- [96] H. Parangusan, D. Ponnamma, M. A. A. Al-Maadeed, *Sci. Rep.* **2018**, *8*, 754.
- [97] Y. Zhou, Y. Liu, M. A. Buckingham, S. Zhang, L. Aldous, S. Beirne, G. G. Wallace, J. Chen, *Electrochem. Commun.* **2021**, *124*, 106938.
- [98] E. D. Eastman, *J. Am. Chem. Soc.* **1928**, *50*, 283.
- [99] H. Wang, D. Zhao, Z. U. Khan, S. Puzinas, M. P. Jonsson, M. Berggren, X. Crispin, *Adv. Electron. Mater.* **2017**, *3*, 1700013.
- [100] M. Beidaghi, Y. Gogotsi, *Energy Environ. Sci.* **2014**, *7*, 867.
- [101] D. Zhao, H. Wang, Z. U. Khan, J. C. Chen, R. Gabrielson, M. P. Jonsson, M. Berggren, X. Crispin, *Energy Environ. Sci.* **2016**, *9*, 1450.
- [102] X. Wu, B. Huang, Q. Wang, Y. Wang, *Chem. Eng. J.* **2019**, *373*, 493.
- [103] Z. A. Akbar, J. Jeon, S. Jang, *Energy Environ. Sci.* **2020**, *13*, 2915.
- [104] D. Zhao, A. Martinelli, A. Willfahrt, T. Fischer, D. Bernin, Z. U. Khan, M. Shahi, J. Brill, M. P. Jonsson, S. Fabiano, X. Crispin, *Nat. Commun.* **2019**, *10*, 1093.
- [105] B. Kim, J. Na, H. Lim, Y. Kim, J. Kim, E. Kim, *Adv. Funct. Mater.* **2019**, *29*, 1807549.
- [106] H. Cheng, X. He, Z. Fan, J. Ouyang, *Adv. Energy Mater.* **2019**, *9*, 1901085.
- [107] H. Cheng, J. Ouyang, *Adv. Energy Mater.* **2020**, *10*, 2001633.
- [108] Y. Fang, H. Cheng, H. He, S. Wang, J. Li, S. Yue, L. Zhang, Z. Du, J. Ouyang, *Adv. Funct. Mater.* **2020**, *30*, 2004699.
- [109] X. He, H. Cheng, S. Yue, J. Ouyang, *J. Mater. Chem. A* **2020**, *8*, 10813.
- [110] S. Horike, Q. Wei, K. Kirihara, M. Mukaida, T. Sasaki, Y. Koshiba, T. Fukushima, K. Ishida, *ACS Appl. Mater. Interfaces* **2020**, *12*, 43674.
- [111] X. Wu, N. Gao, X. Zheng, X. Tao, Y. He, Z. Liu, Y. Wang, *ACS Appl. Mater. Interfaces* **2020**, *12*, 27691.
- [112] G. Ma, J. Li, K. Sun, H. Peng, J. Mu, Z. Lei, *J. Power Sources* **2014**, *256*, 281.
- [113] A. Kundu, T. S. Fisher, *Electrochim. Acta* **2018**, *281*, 357.
- [114] T. Li, X. Zhang, S. D. Lacey, R. Mi, X. Zhao, F. Jiang, J. Song, Z. Liu, G. Chen, J. Dai, Y. Yao, S. Das, R. Yang, R. M. Briber, L. Hu, *Nat. Mater.* **2019**, *18*, 608.
- [115] X. Wang, Y.-T. Huang, C. Liu, K. Mu, K. H. Li, S. Wang, Y. Yang, L. Wang, C.-H. Su, S.-P. Feng, *Nat. Commun.* **2019**, *10*, 4151.
- [116] C.-G. Han, X. Qian, Q. Li, B. Deng, Y. Zhu, Z. Han, W. Zhang, W. Wang, S.-P. Feng, G. Chen, W. Liu, *Science* **2020**, *368*, 1091.
- [117] C. Cheng, Y. Dai, J. Yu, C. Liu, S. Wang, S. P. Feng, M. Ni, *Energy Fuels* **2021**, *35*, 161.
- [118] T. Yamada, Y. Hayamizu, Y. Yamamoto, Y. Yomogida, A. Izadi-Najafabadi, D. N. Futaba, K. Hata, *Nat. Nanotechnol.* **2011**, *6*, 296.
- [119] M. Zu, Q. Li, G. Wang, J. H. Byun, T. W. Chou, *Adv. Funct. Mater.* **2013**, *23*, 789.
- [120] J. Peng, I. Witting, N. Geisendorfer, M. Wang, M. Chang, A. Jakus, C. Kenel, X. Yan, R. Shah, G. J. Snyder, M. Grayson, *Nat. Commun.* **2019**, *10*, 5590.
- [121] T. Sun, B. Zhou, Q. Zheng, L. Wang, W. Jiang, G. J. Snyder, *Nat. Commun.* **2020**, *11*, 572.
- [122] S. M. Jung, J. Kwon, J. Lee, K. Shim, D. Park, T. Kim, Y. H. Kim, S. J. Hwang, Y. T. Kim, *ACS Appl. Energy Mater.* **2020**, *3*, 6383.
- [123] N. Cheng, L. Zhang, K. Doyle-Davis, X. Sun, *Electrochem. Energy Rev.* **2019**, *2*, 539.
- [124] Y. Chen, S. Ji, C. Chen, Q. Peng, D. Wang, Y. Li, *Joule* **2018**, *2*, 1242.
- [125] C. S. Kim, H. M. Yang, J. Lee, G. S. Lee, H. Choi, Y. J. Kim, S. H. Lim, S. H. Cho, B. J. Cho, *ACS Energy Lett.* **2018**, *3*, 501.
- [126] B. Weng, R. L. Shepherd, K. Crowley, A. J. Killard, G. G. Wallace, *Analyst* **2010**, *135*, 2779.
- [127] Zhao C., Liu Y., Beirne S., Razal J., Chen J., *Adv. Mater. Technologies* **2018**, *3*, 1800028.



Yuqing Liu received her Ph.D. (2018) and finished her postdoc work as associate researcher (2019) in the Intelligent Polymer Research Institute (IPRI), University of Wollongong, Australia. She is currently an assistant researcher in University of Electronic Science and Technology of China (UESTC). Her research interest is on the fabrication of wearable energy storage and conversion devices (e.g., thermocells, batteries, supercapacitors, etc.), mainly focusing on nanostructured electrode materials, gel electrolyte/electrode interface, and device fabrication via printing techniques.



Hongbo Wang received his Ph.D. degree in Mechanical Design and Theory from Southwest Jiaotong University in 2018. He is now a postdoctor at the University of Electronic Science and Technology of China. His current research interests focus on fundamental principles, fabrication, and application of plasmonic and thermocell devices.



Jun Chen received his Ph.D. in 2003 from School of Chemistry, University of Wollongong, Australia. Prof. Chen is currently appointed as associate dean of Australian Institute for Innovative Materials (AIIM), and Head of Postgraduate Studies of Intelligent Polymer Research Institute (IPRI), University of Wollongong (UOW). His research interests include electrochemistry, catalysis, sustainable energy devices/systems, electro-/biointerfaces, nano/micro-materials, 2D/3D printing, and design and fabrication of smart wearable electronic devices. Professor Chen has been identified as highly cited researchers in Cross Field (2018 and 2020) by Web of Science—Clarivate Analytics.